Fully- and weakly-nonlinear biperiodic traveling waves in shallow water

Hirakawa, Tomoaki
Department of Energy and Environmental Engineering, Kyushu University

Okamura, Makoto
Research Institute for Applied Mechanics, Kyushu University

出版情報：Fluid Dynamics Research. 50 (2), pp.025510-1-025510-30, 2018-01-31. Japan Society of Fluid Mechanics
バージョン：

Fully- and weakly-nonlinear biperiodic traveling waves in shallow water

Tomoaki Hirakawa[1] **& Makoto Okamura**[2]

[1]Department of Energy and Environmental Engineering, Kyushu University, Kasuga 816-8580, Japan

[2]Research Institute for Applied Mechanics, Kyushu University, Kasuga 816-8580, Japan

E-mail: t-hirakawa@riam.kyushu-u.ac.jp

May 2017

Abstract. We directly calculate fully nonlinear traveling waves that are periodic in two independent horizontal directions (biperiodic) in shallow water. Based on the Riemann theta function, we also calculate exact periodic solutions to the Kadomtsev-Petviashvili (KP) equation, which can be obtained by assuming weakly-nonlinear, weakly-dispersive, weakly-two-dimensional waves. To clarify how the accuracy of the biperiodic KP solution is affected when some of the KP approximations are not satisfied, we compare the fully- and weakly-nonlinear periodic traveling waves of various wave amplitudes, wave depths, and interaction angles. As the interaction angle θ decreases, the wave frequency and the maximum wave height of the biperiodic KP solution both increase, and the central peak sharpens and grows beyond the height of the corresponding direct numerical solutions, indicating that the biperiodic KP solution cannot qualitatively model direct numerical solutions for $\theta \lesssim 45^\circ$. To remedy the weak two-dimensionality approximation, we apply the correction of Yeh et al. [1] to the biperiodic KP solution, which substantially improves the solution accuracy and results in wave profiles that are indistinguishable from most other cases.

PACS numbers: 76B15

Keywords: Shallow water waves, Kadomtsev-Petviashvili (KP) equation, Short-crested waves, Long-crested waves Submitted to: *Fluid Dyn. Res.*

1. Introduction

We consider herein the simplest two-dimensional traveling gravity water waves, which are doubly periodic in two independent horizontal directions. In this paper, we call waves that have two-dimensional wave patterns two-dimensional waves. Accounting for two dimensions is important because real water waves are inherently two-dimensional

rather than one-dimensional. Biperiodic waves can occur when periodic waves propagating different directions intersect each other, or when waves reflect from a vertical wall and interact with incident waves. However, obtaining reasonable numerical solutions that describe fully-nonlinear fundamental water waves (i.e., direct numerical solutions) remains a challenge when the nonlinearity is strong. Studies that search for direct numerical solutions have developed enhanced calculation methods, and are motivated by finding limiting wave profiles [2, 3], harmonic resonances [2, 4, 5], instabilities [6, 7], the pressure exerted on a vertical wall [4, 8, 9], or the departures from weakly-nonlinear solutions [7].

Many studies have used perturbation techniques to obtain a solution to the fundamental water wave equations. This approach involves expanding solutions as a power series in the small parameter ε (see, for example, [10], in which a third-order perturbation solution is calculated for a finite water depth). However, perturbation techniques often suffer from the following four limitations: (i) The radius of convergence of solutions is smaller than the maximum wave amplitude. (ii) If the fundamental mode $(j, k) = (1, 1)$ is assumed, which implies that higher Fourier modes can only be generated at higher orders, the solutions cannot represent harmonic resonant solutions consisting of higher Fourier modes of the same order with the fundamental mode. (iii) If the waves form a nearly one-dimensional wave profile (long-crested waves), the Fourier modes related to the direction perpendicular to the propagation direction slowly decrease with increasing wave number. Such waves occur when two waves propagating in almost the same direction interact strongly with each other. (iv) In shallow water, the wave width narrows and thus requires higher Fourier modes.

Using a semi-analytic approach, Roberts [5] devised an algorithm to perform the perturbation technique that enables to calculate 27th high order perturbation solutions. Furthermore, he applied the Padé approximation to accelerate convergence of the solutions. Marchant and Roberts [8] generalized this algorithm to the finite-depth case and obtained the 32nd order solutions.

Nicholls and Reitich [11] pointed out the above semi-analytic algorithms suffer from numerical instability at high order due to subtle but significant cancellations. They furthermore provided a new, stable high-order perturbation algorithm based on a work of Nicholls and Reitich [12] which describes that a change of variables prior to the perturbation expansion succeeds as it implicitly accounts for all significant cancellations.

The collocation method in space and time has been an effective method and can be implemented on computer in a straightforward manner. Roberts and Schwartz [13], and Okamura [14] calculated truncated double Fourier series solutions on infinite depth by using the collocation method. However, if the waves form sharp peaks, derivatives of the free-surface displacement with respect to space become discontinuous, thus causing severe numerical error. To treat this problem, Tsai and Jeng [15] invoked a kinematic condition that does not involve the derivative of the free-surface displacement η. Recently, Okamura [2] used Galerkin's method to obtain large-amplitude solutions for an infinite depth based on truncated double Fourier series with the kinematic condition

[15], thereby avoiding evaluation of any spatial derivatives of η and thus decreasing the numerical error.

Our primary interest is in the Kadomtsev-Petviashvili (KP) equation which is a weakly-nonlinear equation for shallow water waves and known to have biperiodic solutions involving the Riemann theta function (i.e., KP solutions of genus-2, hereinafter referred to as biperiodic KP solution) [16]. By assuming weak two-dimensionality, the KP equation can be derived by extending the Korteweg-de Vries (KdV) equation, so that the two equations share most of their assumptions. A singly periodic solution to the KP or KdV equation can be written as a Jacobian elliptic function.

Dubrovin [17] and Nakamura [18] proved that the Riemann theta function satisfies the KP equation, provided that the parameters satisfy certain relations. Segur and Finkel [19] presented practical ways to construct this biperiodic KP solution, gave explicit relations that solution parameters must satisfy, and conjectured that biperiodic KP solution represents typical two-dimensional periodic wave phenomena on shallow water. Akylas [20] shows an aerial photograph of real shallow water wave patterns, which supports this conjecture. Motivated by this conjecture, Hammack [21] compared wave patterns of biperiodic KP solution against experimental results obtained in a water pool. The biperiodic KP solution describes the measured waves with reasonable accuracy, even beyond the putative range of the KP theory.

The KP and KdV solutions, which involve Jacobian elliptic functions, and the biperiodic KP solutions all approach solitons as the wavelength approaches infinity. Miles [22] derived a theory for interactions of solitons, finding the resonant interaction regime, that is equivalent to the KP theory; furthermore, he [23] first associated this resonant interaction with the Mach reflection. By comparing the KP soliton with the KdV soliton, Yeh et al. [1] and Li et al. [24] clarified and corrected a deficiency that the KP soliton becomes unphysical when two such solitons propagate in significantly different directions. In addition, the corrected Miles theory and KP theory agree more strongly with numerical [25, 26] and experimental results of solitons [1], although this correction has yet to be applied to KP periodic solutions.

Comparing numerical solutions to the KP equation and the second-order fundamental water wave equation obtained by Bryant [7] suggests that the former solutions (biperiodic KP solutions) differ significantly from the latter ones in both wave height and wave frequency for large angles between the propagation directions of the two incident waves. By using biperiodic KP solution and direct numerical solutions to the fully-nonlinear fundamental water wave equations, we can more precisely understand how the accuracy of biperiodic KP solution varies with increasing wave height a, interaction angle θ, and water depth D.

In this study, we first generalize the method introduced by Okamura [2] to finite water depth and then compare biperiodic KP solution with numerical solutions to fully nonlinear fundamental water wave equations to study the accuracy of biperiodic KP solution for various parameter values. Next, we apply the correction of Yeh et al. [1] to biperiodic KP solution to investigate its accuracy for the wave frequency, the maximum

wave height, and the wave profiles over all space. However, because we focus on the accuracy of biperiodic KP solution and the applicability of the correction, we do not discuss its stability. The sections are organized as follows: In section 2, we generalize the method of Okamura [2] to the case of finite water depth. In section 3, we introduce the KP theory and a method to calculate biperiodic KP solutions. In section 4, we first study the Fourier modes of direct numerical solutions to verify their accuracy, and then compare wave frequencies and maximum wave heights of direct numerical solutions and biperiodic KP solution with varying wave height, interaction angle, and water depth. We next compare wave heights over all space by using the normalized root-mean-square. Finally, we apply the correction of Yeh et al. [1] to biperiodic KP solutions. The results are summarized in section 5.

2. Formulation of direct numerical solutions

We use a Cartesian coordinate system (x, y, z) in which x and y are the horizontal coordinates, and z increases upward. We consider the three-dimensional irrotational flow of an inviscid and incompressible fluid bounded below at flat bottom $z = -h$ and above by a free-surface $z = \eta(x, y, t)$. Since the flow is assumed to be irrotational, a velocity potential $\phi(x, y, z, t)$ exists such that $\mathbf{v} = \nabla\phi$ where $\mathbf{v}$ is the fluid velocity, and $\nabla = (\partial/\partial x, \partial/\partial y, \partial/\partial z)$ is the vector differential operator. The fully-nonlinear water wave equations that govern $\eta(x, y, t)$ and $\phi(x, y, z, t)$ consist of Laplace's equation

$$\Delta\phi = 0 \quad \text{for} \quad -h \leq z \leq \eta(x, y, t), \tag{1}$$

with the bottom condition

$$\phi_z = 0 \quad \text{on} \quad z = -h, \tag{2}$$

the dynamic boundary condition

$$\rho(x, y, z, t) = \phi_t + \beta + \frac{1}{2}\nabla\phi \cdot \nabla\phi + gz = 0 \quad \text{on} \quad z = \eta(x, y, t), \tag{3}$$

and the kinematic boundary condition

$$\frac{D}{Dt}\rho\left(x, y, z, t\right) = 0 \quad \text{on} \quad z = \eta(x, y, t), \tag{4}$$

where $\Delta = \nabla \cdot \nabla$ is the Laplacian, subscripts denote partial derivatives, g is the acceleration due to gravity in the negative z direction, β is an arbitrary constant that is necessary to determine the mean water depth, and $D/Dt = (\partial/\partial t + \nabla\phi \cdot \nabla)$ is the Lagrangian derivative operator. (4) is obtained by applying D/Dt to (3), describing that there is no change of the pressure on a fluid parcel at the free-surface with time, as it follow along its trajectory [2, 15, 27]. Since it is not obvious that (4) can be replaced with the usual kinematic condition: $Df/Dt = 0$ where $f(x, y, z, t) = z - \eta(x, y, t) = 0$ on the free-surface $z = \eta$, we show the derivation of (4) in the following. Noting that the pressure on the free-surface is constant along the free-surface, we have

$$0 = \frac{D_2}{D_2 t}\rho\left(x, y, \eta, t\right) = \left\{\frac{D\rho}{Dt} + \rho_z\left(\eta_t + \nabla_2\phi \cdot \nabla_2\eta - \phi_z\right)\right\}_{z=\eta(x,y,t)}, \tag{5}$$

where $D_2/D_2t = (\partial/\partial t + \nabla_2\phi \cdot \nabla_2)$ and $\nabla_2 = (\partial/\partial x, \partial/\partial y)$. (5) means (4) is equivalent to the usual kinematic condition $\eta_t + \nabla_2\phi \cdot \nabla_2\eta - \phi_z = 0$ on the free-surface $z = \eta$ when $\rho_z \neq 0$. (4) is useful for numerically obtaining limiting waves with sharp crests because it contains no spatial derivatives of the wave height η.

We introduce the following dimensionless quantities and moving coordinate system, assuming waves propagate in the x direction without change in the form:

$$\begin{aligned} &T = \kappa_x x - \omega t, \quad Y = \kappa_y y, \quad Z = \kappa z, \quad H(T,Y) = \kappa\eta(x,y,t), \quad D = \kappa h, \\ &\Phi(T,Y,Z) = \frac{\kappa^2}{\omega}\left(\phi - \frac{\omega}{\kappa_x}x + \frac{\omega^2}{{\kappa_x}^2}t\right), \quad G = \frac{\kappa}{\omega^2}g, \quad B = \frac{\kappa^2}{\omega^2}\beta, \end{aligned} \tag{6}$$

where κ is the wavenumber of the incident wave, ω is the wave frequency, and defining $(p,q) = (\sin\theta, \cos\theta)$, $(\kappa_x, \kappa_y) = (\kappa p, \kappa q)$ is the wavenumber vector of biperiodic waves. In this paper, we will refer to θ as "the interaction angle". (1)-(4) are transformed according to (6) as follows:

$$p^2\Phi_{TT} + q^2\Phi_{YY} + \Phi_{ZZ} = 0 \quad \text{for} \quad -D \le Z \le H, \tag{7}$$

$$\Phi_Z = 0 \quad \text{on} \quad Z = -D, \tag{8}$$

$$P(T,Y,H) = B + \frac{1}{2}\left(p^2\Phi_T^2 + q^2\phi_Y^2 + \phi_Z^2 - p^{-2}\right) + GH = 0 \quad \text{on} \quad Z = H, \tag{9}$$

$$\begin{aligned} Q(T,Y,H) =& p^2\Phi_T\left(p^2\Phi_T\Phi_{TT} + q^2\Phi_Y\Phi_{TY} + \Phi_Z\Phi_{TZ}\right) \\ &+ q^2\Phi_Y\left(p^2\Phi_T\Phi_{TY} + q^2\Phi_Y\Phi_{YY} + \Phi_Z\Phi_{YZ}\right) \\ &+ \Phi_Z\left(p^2\Phi_T\Phi_{TZ} + q^2\Phi_Y\Phi_{YZ} + \Phi_Z\Phi_{ZZ} + G\right) = 0 \quad \text{on} \quad Z = H. \end{aligned} \tag{10}$$

We look for a periodic and symmetric solution Φ in the form

$$\begin{aligned} \Phi = -\frac{1}{p^2}T + \sum_{k=0}^{N}\sum_{j=1}^{N} A_{j,k}\left[\cosh(\alpha_{j,k}Z) + \sinh(\alpha_{j,k}Z)\tanh(\alpha_{j,k}D)\right]\cos(kY)\sin(jT), \\ \alpha_{j,k} = \sqrt{k^2q^2 + j^2p^2}. \end{aligned} \tag{11}$$

If $k + j$ is odd, $A_{j,k}$ is always zero, so that the number of unknowns $A_{j,k}$ is reduced to $N(N+1)/2$, and N is the truncation number. The quantities B and G are also unknown. It is important to note that the formulation using Φ in the present paper is consistent with that using $\widetilde{\Phi} = \Phi + T/p^2$ in Okamura [2].

2.1. Computational method

By applying Galerkin's method, we obtain the independent relations

$$\begin{aligned} F_{l,m}(A_{j,k}, B, G) = \int_0^\pi dT \int_0^\pi dY Q(T,Y,H; A_{j,k}, B, G)\cos(lY)\sin(mT) \\ \text{on} \quad Z = H(T,Y), \end{aligned} \tag{12}$$

which is two-dimensional Fourier transform of n-points with respect to T and Y. The truncation number N in (11) and n are set $(N,n) = (50,64)$ unless otherwise mentioned. We impose the following independent relation so that D becomes the mean fluid depth:

$$s(A_{j,k}, B, G) = \int_0^\pi dT \int_0^\pi dY H(T,Y; A_{j,k}, B, G) = 0, \tag{13}$$

which is numerically evaluated by using the trapezoidal rule. Another independent relation is expressed as

$$\Pi(A_{j,k}, B, G) = \varepsilon D - H\left(\frac{\pi}{2}, \frac{\pi}{2}; A_{j,k}, B, G\right) + H(\pi, 0; A_{j,k}, B, G) = 0, \quad (14)$$

where ε is a parameter of the nonlinearity. The wave height $H(T, Y)$ usually has a maximum at $T = Y = 0$ where two periodic waves superimpose and interact with each other, whereas $H(T, Y)$ has the minimum at $T = \pi$ and $Y = 0$ (see figure 1). The wave height $H(\pi/2, \pi/2)$ corresponds to the crest of a periodic waves; hence, the interaction between the two waves is very weak. In the case of the soliton-like wave, εD almost corresponds to the soliton amplitude, and using (14) makes it easy to evaluate the amplitude of one of periodic waves that construct a biperiodic wave and the weakly nonlinear approximation of KP. Note that instead of using ε in (14), the wave steepness ϵ defined as $2\epsilon - H(0,0) + H(\pi, 0) = 0$ is often used in studies of short-crested wave.

Newton's method is used to find $A_{j,k}$, B, and G from (12)-(14). Note that the wave height $H(T, Y)$ is evaluated at every Newton iteration by solving (9) and substituted into these equations (for the detailed procedure, see [2]). The third-order short-crested wave obtained by Hsu et al. [10] is used as the initial solution of the iterations, and we stop the iteration when the maximum difference between wave heights before and after a given iteration is less than 10^{-10}. Solutions that do not satisfy (10) for $Q < 10^{-4}\varepsilon$ are excluded from the results. Finally, the Jacobian matrix, which is necessary for Newton's method, is calculated in Appendix A.

3. KP theory

The KP equation can be written in the dimensional form:

$$\left(\eta_t + c_s\eta_x + \frac{3c_s}{2h}\eta\eta_x + \frac{c_s h^2}{6}\eta_{xxx}\right)_x + \frac{c_s}{2}\eta_{yy} = 0, \quad (15)$$

where $c_s = \sqrt{gh}$ which denotes the phase velocity in shallow water. The KP equation can be derived from the fully-nonlinear water wave equations (1)-(4) under the following four approximations:

$$|\eta|_{\max}/h \ll 1, \quad \kappa h \ll 1, \quad \kappa_y/\kappa_x \ll 1, \quad O\left(|\eta|_{\max}/h\right) \simeq O\big((\kappa h)^2\big) = (\kappa_y/\kappa_x)^2, \quad (16)$$

which respectively means weak nonlinearity, weak dispersivity, weak two-dimensionality approximation, and the strengths of these three have comparable influence. Note that $(|\eta|_{\max}/h, \kappa h, \kappa_y/\kappa_x)$ correspond to $(H(0,0)/D, D, 1/\tan\theta)$, where $H(0,0)$ is the maximum wave height. To organize results, in stead of $H(0,0)/D$ we use the nonlinear parameter ε defined in (14), because controlling the incident wave height $H(\pi/2, \pi/2) - H(\pi, 0)$ in (14) is easier than controlling the maximum wave height $H(0,0)$ in experiments. Non-dimensional form of (15):

$$(U_{\hat{T}} + 6UU_{\hat{X}} + U_{\hat{X}\hat{X}\hat{X}})_{\hat{X}} + 3U_{\hat{Y}\hat{Y}} = 0, \quad (17)$$

can be obtained by using non-dimensional quantities:

$$U = \frac{3\eta}{2h}, \quad \hat{X} = \frac{x}{h} - \frac{c_s}{h}t, \quad \hat{Y} = \frac{y}{h}, \quad \hat{T} = \frac{c_s}{6h}t. \tag{18}$$

Using the Riemann theta function ϑ, the biperiodic KP solution can be written in the form

$$U\left(\hat{X}, \hat{Y}, \hat{T}\right) = 2\left[\ln \vartheta\left(\Theta_1, \Theta_2; \mathbf{B}\right)\right]_{\hat{X}\hat{X}}, \tag{19}$$

where

$$\vartheta\left(\Theta_1, \Theta_2; \mathbf{B}\right) = \sum_{m_1=-\infty}^{\infty} \sum_{m_2=-\infty}^{\infty} \exp\left[\frac{1}{2}\mathbf{m}^{\mathsf{T}} \cdot \mathbf{B} \cdot \mathbf{m} + \mathrm{i}\mathbf{m}^{\mathsf{T}} \cdot \mathbf{Q}\right],$$
$$\Theta_i = M_i\hat{X} + N_i\hat{Y} + \Omega_i\hat{T} + \pi,$$
$$\mathbf{m} = \begin{pmatrix} m_1 \\ m_2 \end{pmatrix}, \quad \mathbf{B} = \begin{pmatrix} b & b\lambda \\ b\lambda & b\lambda^2 - d \end{pmatrix}, \quad \mathbf{Q} = \begin{pmatrix} \Theta_1 \\ \Theta_2 \end{pmatrix},$$
$$b < 0, \quad \lambda^2 \leq \frac{1}{2}, \quad d \leq b(1-\lambda^2),$$

where i is the imaginary number, and the mean wave height is always zero. A superscript T denotes the matrix transpose operation. Dubrovin [17] and Nakamura [18] prove that $U(\hat{X}, \hat{Y}, \hat{T})$ satisfies (17), provided that its eleven parameters satisfy certain relations. Segur and Finkel [19] give explicit relations that eleven parameters of the solution must satisfy. Assuming symmetric wave interactions, we reduced the relations involving eleven parameters to a relation involving just two parameters b and λ:

$$\Omega_1(b, \lambda) = \Omega_2(b, \lambda), \tag{20}$$

which corresponds to (12) (see Appendix B for details). We introduce the free-surface displacement of a traveling wave U^* on the moving coordinate system T^*:

$$U^*\left(T^*, \hat{Y}; b, \lambda\right) = U\left(\hat{X}, \hat{Y}, \hat{T}; b, \lambda\right), \quad T^* = \hat{X} + \frac{\Omega_1}{M_1}\hat{T}. \tag{21}$$

The wave height $H_{\mathrm{KP}}(T, Y; b, \lambda)$ of the KP solution is expressed by

$$H_{\mathrm{KP}}\left(T, Y; b, \lambda\right) = \frac{2D}{3} U^*\left(\frac{T}{M_1}, \frac{Y}{N_1}; b, \lambda\right), \tag{22}$$

where D is the non-dimensional mean water depth in (6). Another independent relation is

$$\varepsilon D - H_{\mathrm{KP}}\left(\frac{\pi}{2}, \frac{\pi}{2}; b, \lambda\right) + H_{\mathrm{KP}}\left(\pi, 0; b, \lambda\right) = 0, \tag{23}$$

which corresponds to (14). We solve (20) and (23) for b and λ using Newton's method. Using a fast convergent theta function is crucially important to find a root and increase the solution accuracy. Three different forms of theta functions are introduced in (4.7), (4.19a), and (4.19b) of Segur and Finkel [19], which are equivalent but have different convergence speeds with respect to the number of terms after which the sum is truncated. The convergence speeds of these functions mainly depend on b and λ in the case of symmetric waves. We use theta function of (4.19b) of Segur and Finkel [19] for $b \geq 5$;

otherwise, we use (4.7) of Segur and Finkel [19]. (4.19a) may not be important for symmetric waves. The upper and lower limits of the theta functions are set to $m_{\max} = 5$ and $m_{\min} = -5$, respectively. Solutions (b, λ) satisfy (23) to an accuracy of at least $10^{-5}\varepsilon$.

Here, as b approaches zero, the effective wave width gets shorter, and the wave becomes solitons in the limit $b \to 0$. For symmetric waves, λ determines the difference between the interaction angle θ and another angle θ^*, which decides lines that wave crests lie along:

$$\tan\theta^* = \frac{1-\lambda}{1+\lambda}\tan\theta, \quad \lambda^2 \leq \frac{1}{2}. \tag{24}$$

The difference between θ and θ^* reflects how strongly the two waves affect each other in an oblique interaction. Figure 1 presents a schematic diagram that shows the difference between θ and θ^*.

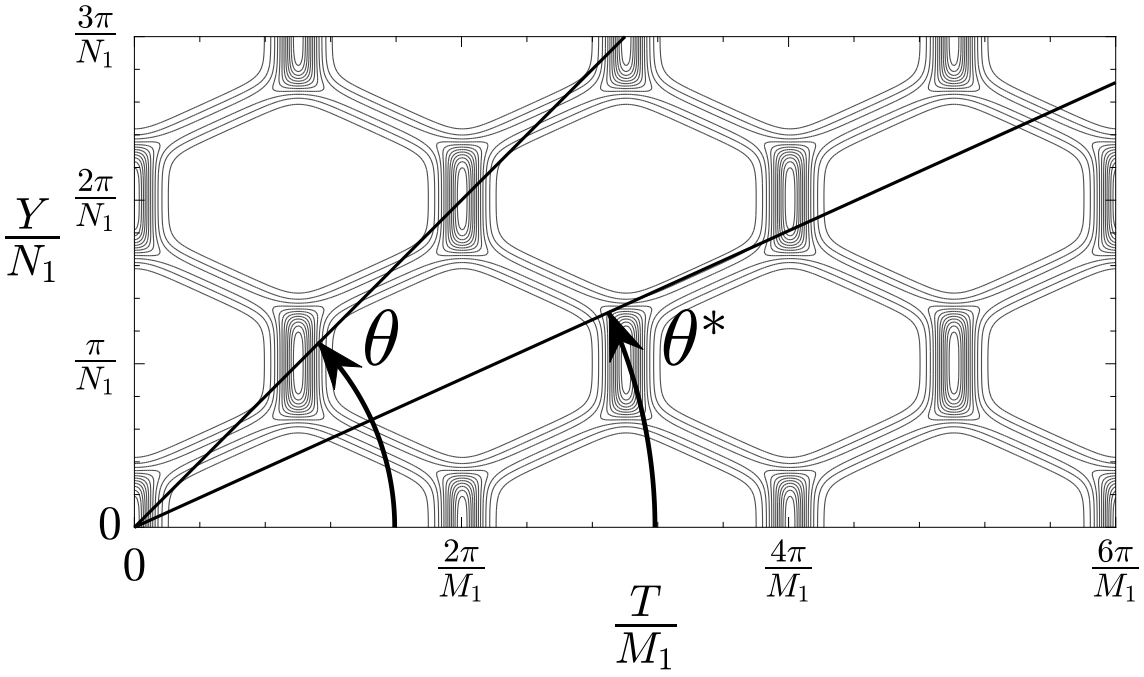

Figure 1. Contour plot of wave patterns of biperiodic KP solution when long stems occur with the interaction angle θ and the other angle θ^* which decides lines that wave crests lie along. $\lambda = 0$ implies no oblique interaction.

4. Results and Discussion

For short-crested waves, setting the wave numbers $(j, k) = (1, 1)$ for the linear solution an higher harmonic becomes infinite when a certain set of (D, θ) satisfies a relation:

$$\alpha_{j,k}\tanh\left(\alpha_{j,k}D\right) = j^2\tanh\left(D\right), \tag{25}$$

which implies that the higher harmonic is resonated with the linear wave of $(j,k) = (1,1)$, that is the order of the higher harmonic is inappropriate. Sometimes direct numerical solutions are affected by harmonic resonances, although we find no resonance in KP solutions. In particular, as the wave amplitude ε increases, direct numerical solutions tend to be strongly affected by harmonic resonances. Therefore, we compare the direct numerical solution and biperiodic KP solutions for $\varepsilon \leq 0.1$. Note that, even for $\varepsilon = 0.1$, wave heights at the peak $H(0,0)/D$ can exceed 0.3. We denote by A-I cases involving the parameters $(\varepsilon, \theta) = (0.1, 45^\circ)$, $(0.05, 45^\circ)$, $(0.01, 45^\circ)$, $(0.1, 59.5^\circ)$, $(0.05, 59.5^\circ)$, $(0.01, 59.5^\circ)$, $(0.1, 69.5^\circ)$, $(0.05, 69.5^\circ)$, and $(0.01, 69.5^\circ)$, respectively. For cases A-I, the mean water depth is fixed at $D = 2\pi/50$ so that the KP approximation of weak dispersivity is satisfied. In this section, we compare and analyze in detail solutions for cases A-I. In section 4.1, we check the Fourier modes of direct numerical solutions $|A_{j,k}|$ for cases A-I to verify their accuracy. To clarify how the accuracy of the biperiodic KP solution varies when the two KP approximations are not satisfied (i.e., weak nonlinearity and weak two-dimensionality), section 4.2 compares both wave frequencies and maximum wave heights of solutions with varying parameters ε, θ, and D. Section 4.3 makes a qualitative comparison of the wave height over the whole space between solutions. Finally, section 4.4 confirms the correction [1] for biperiodic KP solutions.

4.1. Fourier mode analysis

In this section, we analyze the amplitudes of Fourier modes $|A_{j,k}|$ of the direct numerical solutions for cases A-I to verify their accuracy. Figure 2 shows the amplitudes $\log|A_{j,k}|$ for cases A-I. When ε is relatively small (i.e., $\varepsilon = 0.01, 0.05$), the amplitudes $|A_{j,k}|$ rapidly decrease below 10^{-15} before one of the wavenumbers (j,k) reaches the maximum $N = 50$. The amplitude $|A_{j,k}|$ decays more slowly as ε increases, although for $\varepsilon = 0.1$, $|A_{j,k}|$ is sufficiently small ($|A_{j,k}| < 10^{-10}$) for at least one wavenumber to reach the maximum $N = 50$.

Similarly, $|A_{j,k}|$ slowly decreases with increasing θ, thus strengthening the oblique interaction, which implies that the stem length becomes more elongated, and the phase more shifted. For example, figures 3(a) and 3(b) show Fourier modes and a wave profile for the case $(\varepsilon, \theta, D) = (0.01,\ 88^\circ, 2\pi/50)$, which has a larger interaction angle θ than that for the case of figure 2(i). As the oblique interaction increases, $|A_{j,k}|$ becomes more biased and decays more slowly in the direction of the wavenumber k, forming a square wave at the central peaks in the k direction (i.e., a long-crested wave). Such slowly converging solutions cannot be obtained with high accuracy by the perturbation technique with setting $(j,k) = (1,1)$ as the fundamental, because setting $(j,k) = (1,1)$ as the fundamental, implicitly assumes that the higher Fourier modes can be generated at higher orders in the expansions, which evidently contradicts the requirements of a slowly converging solutions. In deep water, for the case $90^\circ - \theta = O(\varepsilon)$, Roberts and Peregrine [28] obtained a long-crested wave solution based on the Jacobian elliptic

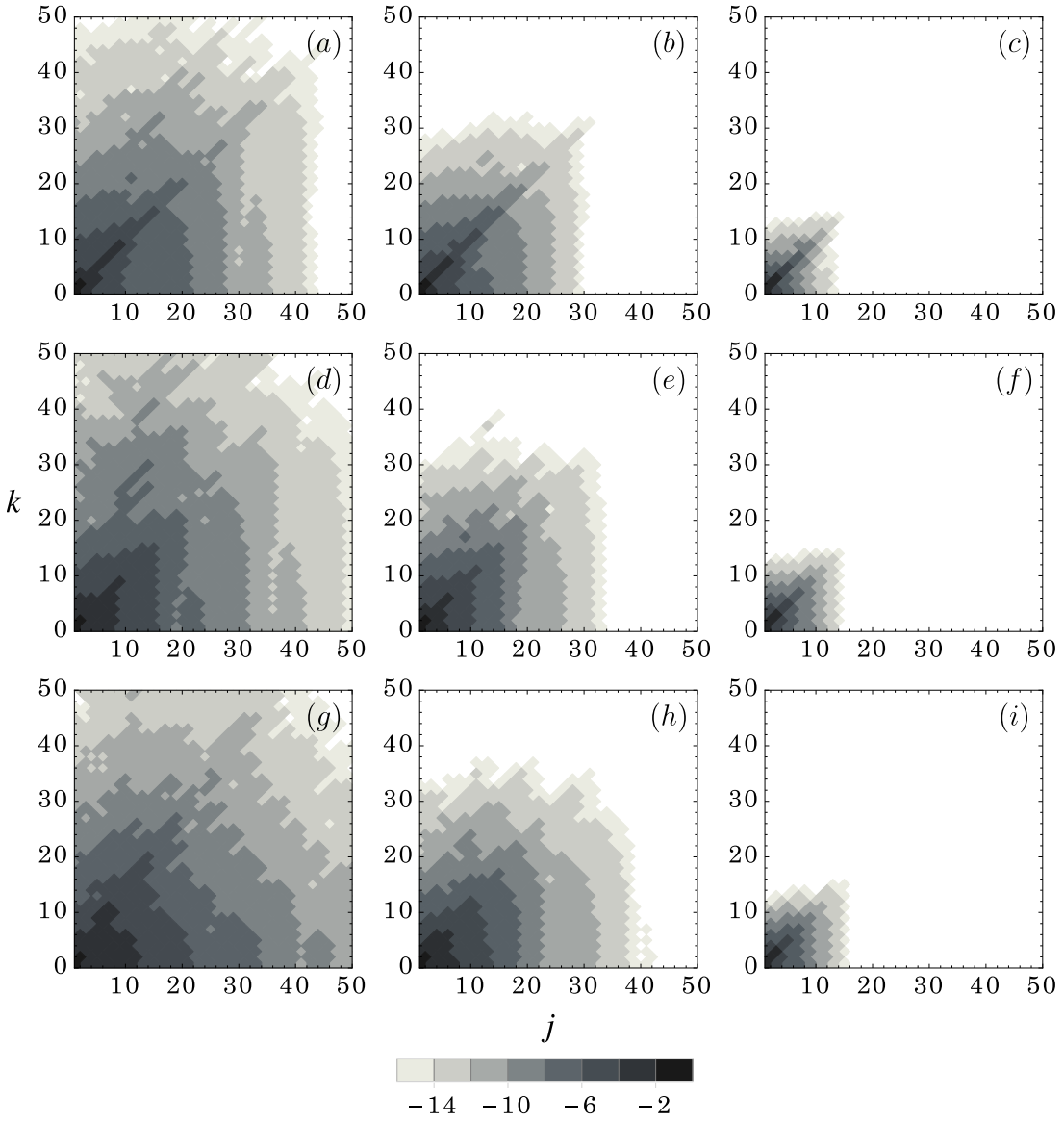

Figure 2. Fourier modes $\log|A_{j,k}|$ divided by wavenumbers j and k for cases A-I where the depth is fixed at $D/2\pi = 1/50$: (a) case A:$(\varepsilon,\theta) = (0.1, 45°)$, (b) B: $(\varepsilon,\theta) = (0.05, 45°)$, (c) C: $(\varepsilon,\theta) = (0.01, 45°)$, (d) D: $(\varepsilon,\theta) = (0.1, 69.5°)$, (e) E: $(\varepsilon,\theta) = (0.05, 69.5°)$, (f) F: $(\varepsilon,\theta) = (0.1, 69.5°)$, (g) G: $(\varepsilon,\theta) = (0.1, 59.5°)$, (h) H: $(\varepsilon,\theta) = (0.05, 59.5°)$, (i) I: $(\varepsilon,\theta) = (0.1, 59.5°)$.

function, which includes higher Fourier modes even in the first order. In the biperiodic KP solution also represents long-crested waves. We thus set the truncation number $N = 50$ in (11) so that most of the solutions converge, even for the case of figure 3, which corresponds to slow decay of the Fourier modes. Moreover, we exclude solutions from the following results when Q in (10) does not satisfy the condition $Q < 10^{-4}\varepsilon$. Note that increasing the mean water depth D presents no problem because wave profiles become smoother sinusoidal waves as D increases.

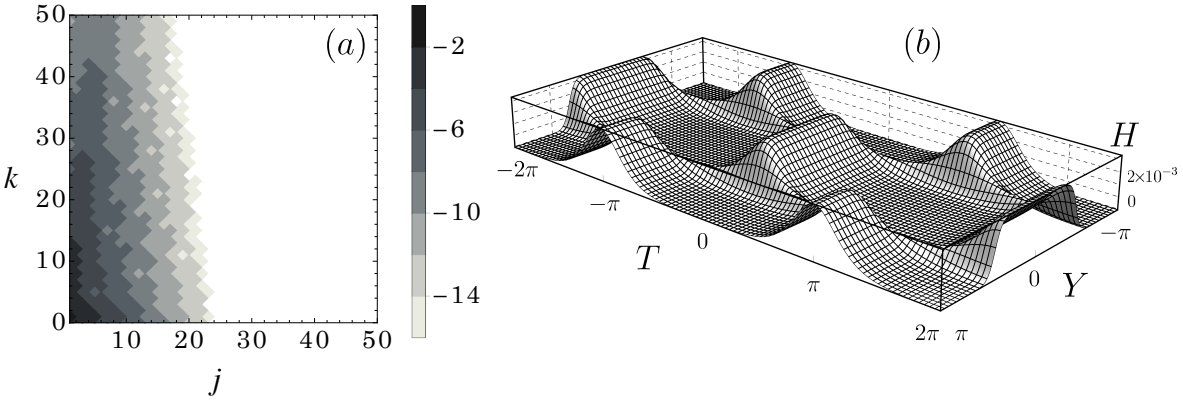

Figure 3. (a) Fourier modes $\log|A_{j,k}|$ divided by wavenumbers j and k, and (b) wave profile of the direct numerical solution for the case $(\varepsilon, \theta, D/2\pi) = (0.01, 88°, 1/50)$, showing that a strong oblique interaction results in long-crested waves with peaks that almost correspond to Mach stems.

4.2. Comparison of W and α for various parameters (ε, θ, D)

In this section, we compare wave frequencies $W = \omega/\omega_0$ and maximum wave heights α of direct numerical solutions and biperiodic KP solutions for various wave amplitudes ε, interaction angles θ, and mean water depths D. Here, W is normalized by the linear wave frequency $\omega_0 = \sqrt{g\kappa\tanh(\kappa h)}$. The wave frequencies W of direct numerical solutions and the biperiodic KP solutions can be written as

$$W_{\rm dir} = \frac{1}{\sqrt{G\tanh D}}, \quad W_{\rm KP} = \sqrt{\frac{D}{\tanh D}}\left(p - \frac{\Omega_1}{6D}\right), \tag{26}$$

where Ω_1 is given in Appendix B. The maximum wave heights α of direct numerical solutions and of biperiodic KP solutions are written as

$$\alpha_{\rm dir} = \frac{H(0,0)}{\varepsilon D}, \quad \alpha_{\rm KP} = \frac{H_{\rm KP}(0,0)}{\varepsilon D}. \tag{27}$$

We first focus on the effects of weak nonlinearity and weak two-dimensionality, setting the mean water depth $D = 2\pi/50$ so that weak dispersivity is satisfied. Note that $(|\eta|_{\max}/h, \kappa_y/\kappa_x, \kappa h)$ in (16) correspond to $(\varepsilon\alpha, 1/\tan\theta, D)$.

Figures 4(a) and 4(b) respectively compare W and α values of direct numerical solutions with those of the biperiodic KP solutions while varying the nonlinearity parameter ε and the interaction angle θ. Table 1 compares W and α for cases A-I in more detail. The biperiodic KP solution cannot be obtained for angles θ larger than those shown in figures 4(a) and 4(b) because θ reaches the limit of the range in which a symmetric biperiodic KP solution can exist, which will become clear in section 4.4 upon checking the parameter λ.

The biperiodic KP solution is consistent with the direct numerical solutions for both W and α for small ε and large θ, which satisfies (16). Even for ε as small as 0.01, W

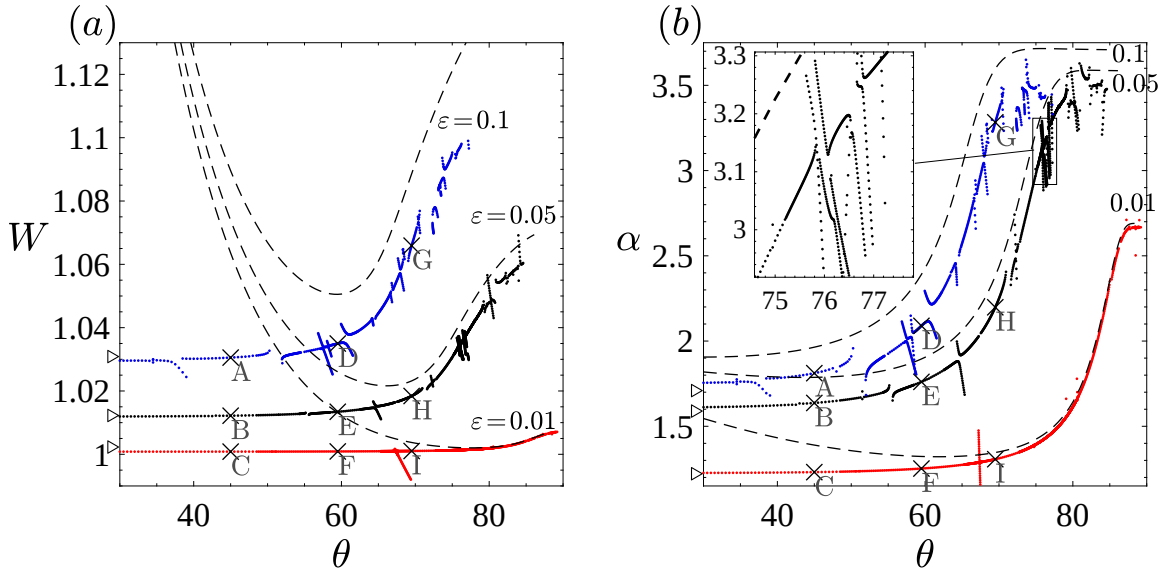

Figure 4. Direct solutions (dots) and biperiodic KP solutions (dashed lines) for $\varepsilon = 0.01$ (bottom), 0.05 (middle) and 0.1 (top), showing the dependence of (a) wave frequency W and (b) maximum wave height α on θ. The symbols $\times$ describe direct numerical solutions of cases A-I, and the symbols $\triangleright$ on the vertical axis indicate superposition of periodic KdV solutions involving the Jacobian elliptic function. Note that α differs slightly between the superposition of periodic KdV solutions and the direct numerical solutions, which may be due to the difference between single periodicity and double periodicity, and the strong nonlinearity involved in direct numerical solutions for large ε.

Table 1. For cases A-I, wave frequencies $W_{\rm dir} - 1$ of direct numerical solutions, wave frequencies $W_{\rm KP} - 1$ of biperiodic KP solutions, maximum wave heights $\alpha_{\rm dir}$ of direct numerical solutions, maximum wave heights $\alpha_{\rm KP}$ of biperiodic KP solution, differences $W_{\rm KP}/W_{\rm dir} - 1$ between $W_{\rm dir}$ and $W_{\rm KP}$, and differences $\alpha_{\rm KP}/\alpha_{\rm dir} - 1$ between $\alpha_{\rm dir}$ and $\alpha_{\rm KP}$.

θ	ε	Case	$W_{\rm dir} - 1$	$W_{\rm KP} - 1$	$\alpha_{\rm dir}$	$\alpha_{\rm KP}$	$\frac{W_{\rm KP}}{W_{\rm dir}} - 1$	$\frac{\alpha_{\rm KP}}{\alpha_{\rm dir}} - 1$
	0.1	A	3.06×10^{-2}	8.96×10^{-2}	1.81	1.96	5.73×10^{-2}	8.41×10^{-2}
45°	0.05	B	1.22×10^{-2}	7.39×10^{-2}	1.64	1.79	6.10×10^{-2}	9.18×10^{-2}
	0.01	C	8.48×10^{-4}	6.36×10^{-2}	1.23	1.39	6.27×10^{-2}	1.29×10^{-1}
	0.1	D	3.50×10^{-2}	5.05×10^{-2}	2.09	2.39	1.50×10^{-2}	1.44×10^{-1}
59.5°	0.05	E	1.34×10^{-2}	2.61×10^{-2}	1.76	1.89	1.24×10^{-2}	7.62×10^{-2}
	0.01	F	9.00×10^{-4}	1.31×10^{-2}	1.25	1.32	1.22×10^{-2}	5.66×10^{-2}
	0.1	G	6.59×10^{-2}	8.86×10^{-2}	3.28	3.60	2.13×10^{-2}	9.59×10^{-2}
69.5°	0.05	H	1.84×10^{-2}	2.32×10^{-2}	2.20	2.38	4.67×10^{-3}	8.33×10^{-2}
	0.01	I	1.04×10^{-3}	3.73×10^{-3}	1.31	1.35	2.69×10^{-3}	3.00×10^{-2}

and α for biperiodic KP solutions vary gradually from those for the direct numerical solutions as the slight decrease in θ is too small to satisfy the weak two-dimensionality, such as happens for $\theta = 45°$, and both W and α eventually diverge to infinity at $\theta = 0$,

Table 2. For cases $D/2\pi = 0.05, 0.15, 0.25$: wave frequencies $W_{\rm dir} - 1$ of direct numerical solutions, wave frequencies $W_{\rm KP} - 1$ of biperiodic KP solutions, maximum wave heights $\alpha_{\rm dir}$ of direct numerical solutions, maximum wave heights $\alpha_{\rm KP}$ of biperiodic KP solutions, differences between $W_{\rm dir}$ and $W_{\rm KP}$, $1-W_{\rm KP}/W_{\rm dir}$ and between $\alpha_{\rm dir}$ and $\alpha_{\rm KP}$, $1 - \alpha_{\rm KP}/\alpha_{\rm dir}$.

$\frac{D}{2\pi}$	$W_{\rm dir} - 1$	$W_{\rm KP} - 1$	$\alpha_{\rm dir}$	$\alpha_{\rm KP}$	$1 - \frac{W_{\rm KP}}{W_{\rm dir}}$	$1 - \frac{\alpha_{\rm KP}}{\alpha_{\rm dir}}$
0.05	4.82×10^{-4}	1.78×10^{-4}	1.17	1.17	3.05×10^{-4}	4.45×10^{-3}
0.15	1.31×10^{-4}	-6.78×10^{-3}	1.05	1.04	6.91×10^{-3}	7.47×10^{-3}
0.25	1.14×10^{-4}	-2.23×10^{-1}	1.02	1.01	2.23×10^{-1}	1.47×10^{-2}

which is an apparent shortcoming of the KP equation. Figures 4(a) and 4(b) also show that biperiodic KP solutions deviate from superposition of periodic KdV solutions as θ becomes smaller, whereas direct numerical solutions approach superposition of periodic KdV solutions. In their studies of solitons of the KP equation, Yeh et al. [1] pointed out this shortcoming; moreover, they described how it can be corrected. We discuss this correction in detail in section 4.4.

As the wave amplitude ε and the interaction angle θ increase, the number of visible disconnections increases and bifurcation branches become larger. If we compare biperiodic KP solutions and direct numerical solutions while avoiding bifurcation branches and for the relatively large angle $\theta = 69.5°$, both the maximum wave heights α and the interaction angles θ deviate with increasing ε. For example, for $\theta = 69.5°$, the maximum wave height reaches $\alpha_{\rm dir} = 3.28$ at $\varepsilon = 0.1$ (i.e., $H_{\rm KP}(0,0) = 0.328$, and the wave steepness $\epsilon = 0.164$), results in the large differences, $\alpha_{\rm KP}/\alpha_{\rm dir} - 1 = 9.75 \times 10^{-2}$ and $W_{\rm KP}/W_{\rm dir} - 1 = 2.13 \times 10^{-2}$.

Table 1 shows that $W_{\rm KP}/W_{\rm dir} - 1$ is less than $\alpha_{\rm KP}/\alpha_{\rm dir} - 1$, which indicates that the wave frequency less influenced by the failure of the weak nonlinearity approximation. This is reasonable because the perturbation solution shows that the wave frequency is primarily influenced by the wave amplitude ε at second order, whereas the wave height is primarily influenced at first order. Consequently, the wave height is more sensitive to the nonlinearity than the wave frequency.

Comparing numerical solutions to the KP equation and the second-order fundamental water wave equation obtained by Bryant [7] suggests that values W and α for the former solution are greater than those for the latter ones. This becomes more pronounced with decreasing θ. These tendencies are consistent with the present results.

We next focus on the effects of the failure of the weak dispersivity approximation by setting $(\varepsilon, \theta) = (0.01, 85°)$ so that only weak nonlinearity and weak two-dimensionality are satisfied. Table 2 shows W and α for both direct numerical solutions and for biperiodic KP solutions for the ratio $D/2\pi = 0.05, 0.15, 0.25$ of the mean water depth to the wavelength 2π. Figure 5 shows W and α as a function of the ratio $D/2\pi$. For small water depths $D/2\pi$, the biperiodic KP solutions are in close agreement with the

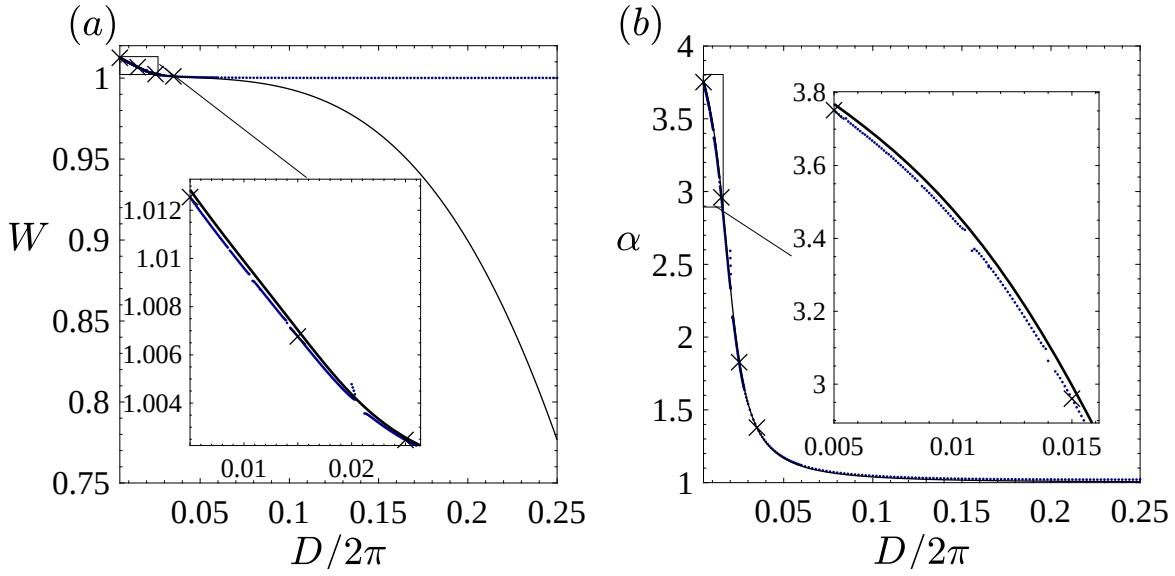

Figure 5. Direct numerical solutions (dots) and biperiodic KP solutions (solid lines) for $(\varepsilon, \theta) = (0.01, 85^\circ)$, showing the dependence of (a) wave frequency W and (b) maximum wave height α on the ratio $D/2\pi$. The truncation number N in (11) and the number of samples n for the fast Fourier transform in (12) are set to $(N, n) = (60, 128)$ for $D/2\pi < 0.01$, and $(N, n) = (50, 64)$ otherwise to obtain solutions that converge adequately and satisfy $Q < 10^{-4}\varepsilon$. The symbols $\times$ are labeled on the direct numerical solutions for $D/2\pi = 1/200, 3/200, 5/200, 7/200$, the wave profiles for which are shown in figure 7.

direct numerical solutions. Although KP solutions are offset a little from the direct numerical solutions, the small discrepancies can be diminished by decreasing ε. Even with ε as small as 0.01, as $D/2\pi$ increases, W and α for the biperiodic KP solutions gradually deviate from the values for the direct numerical solutions, thus violating the weak dispersivity approximation. Interestingly, at the maximum depth studied here (i.e., $D/2\pi = 0.25$), $1 - W_{\mathrm{KP}}/W_{\mathrm{dir}}$ deviates by as much as 2.23×10^{-1}, whereas $1 - \alpha_{\mathrm{KP}}/\alpha_{\mathrm{dir}}$ deviates by only 1.47×10^{-2}.

Although comparing α is simple and important for verifying the accuracy of solutions regarding the wave height, α gives the wave height just at the center point, and not over the whole space. We discuss this point in the next section.

4.3. Comparison of wave heights

To quantify the accuracy of biperiodic KP solutions regarding wave heights over the whole space, we use the normalized root-mean-square (rms) σ, which is a traditional measure of error, to express differences between direct numerical solutions and biperiodic

KP solutions. We defined σ as

$$\sigma^2 = \frac{\displaystyle\int_0^{\pi} dT \int_0^{\pi} dY [H(T,Y) - H_{\mathrm{KP}}(T,Y)]^2}{\displaystyle\int_0^{\pi} dT \int_0^{\pi} dY H(T,Y)^2}. \tag{28}$$

This definition of σ is the same as the one used by Hammack [21] except that sums are replaced by integrals, which are evaluated by the trapezoidal rule to obtain more precise values. The truncation number for the trapezoidal rule are set sufficiently large so as not to affect σ by more than 10^{-5}. The value $\sigma = 0$ leads to a perfect agreement of results, and $\sigma = 1$ is equivalent to using no theory at all.

For cases A-I, σ is 2.54×10^{-1}, 2.40×10^{-1}, 1.68×10^{-1}, 1.34×10^{-1}, 1.09×10^{-1}, 6.49×10^{-2}, 1.56×10^{-1}, 6.45×10^{-2}, and 2.73×10^{-2}, respectively. As expected, σ mostly increases with increasing ε and θ, which is well predicted by α in the previous section. However, some discrepancies exist between the tendency of σ and α: for example, for case C, σ is relatively small, unlike the value of $\alpha_{\mathrm{KP}}/\alpha_{\mathrm{dir}} - 1$ (see table 1), suggesting that σ should be used to more precisely judge the accuracy.

Bryant [7] shows that the central peaks of the biperiodic KP solutions are sharper and higher than those of the corresponding solutions to second-order fundamental water wave solution, and this feature becomes more pronounced with decreasing θ. For cases A-I of the present results, cross sections through the central peak in the Y direction show the same tendency. Similarly, we study a cross section through the central peak in the T direction so that we can observe a stem, which reflects the intensity of the oblique interaction. Figure 6 compares cross sections in the T direction and over a range $-\pi/2 \leq Y \leq \pi/2$ of the direct numerical solutions and the biperiodic KP solutions.

As expected from the result of table 1, for case I, cross sections in the T direction match each other well. For relatively large angles, as θ decreases, the central peak of biperiodic KP solutions tends to be sharper and higher than that of the corresponding direct numerical solutions, which is similar to the situation for cross sections in the Y direction. This result clearly indicates that biperiodic KP solutions cannot model direct numerical solutions in both qualitatively and quantitatively when θ is too small to satisfy KP approximation (16). This clarifies the deficiency in appearence of biperiodic KP solutions that corresponds to their deviations in figure 4(b).

For relatively small angles, as θ increases, the central peaks of both the direct numerical solutions and biperiodic KP solution become stems elongated in the Y direction, indicating that their phases are similarly shifted by the strong oblique interaction. Stems of solutions grow even longer and higher as θ increases, thus transforming their shapes into one-dimensional waves. (see figure 3 for an example).

For the case $\theta = 45°, 59.5°$, as ε increases, the central peaks of the biperiodic KP solutions tend to become sharper and higher than those of the corresponding direct numerical solutions. For example, σ surprisingly reaches 2.54×10^{-1} for case A. This discrepancy is caused by the failure of both the weak nonlinearity and the weak two-dimensionality approximations. Studying wave troughs at $T = \pi/2$ in figure 6, we see

that, as the wave amplitude ε increases, a soliton lump forms as the effective width decreases and the wave troughs flatten. This intuitive assertion is proved by verifying that parameter b approaches 0, because the biperiodic KP solution matches with KP two-soliton in the limit $b \to 0$.

We next examine how σ changes upon varying the mean water depth D. For $D = \pi/10, 3\pi/10, 5\pi/10$ with $\varepsilon = 0.01$, we calculate $\sigma = 4.08662 \times 10^{-3}$, 6.51459×10^{-3}, and 1.07203×10^{-2}. The result for σ slightly increases with increasing D, when the biperiodic KP solution violates the weak dispersivity approximation. In most of these cases, profiles of the biperiodic KP solutions are virtually indistinguishable from those of direct numerical solution. For example, profiles of direct numerical solutions labeled by the symbol $\times$ in figure 5 are plotted in figures 7(a)-7(d). From these examples, we can see how a solitary wave lump evolves as the water depth D decreases.

4.4. Correction for weak two-dimensionality approximation

For solitons, Yeh et al. [1] shows the deficiency can be corrected within the framework of the KP theory by representing the wave amplitude as $\varepsilon \sin^2 \theta^*$ instead of the measured wave amplitude ε. In this section, we check whether this can be applied to a periodic traveling wave by replacing solitons in Yeh et al. [1] with periodic solutions.

The KdV equation describes one-dimensional propagating waves with weak quadratic nonlinearity and weak dispersion. Both KdV and KP equations accept the one-dimensional periodic solution of the Jacobian elliptic function (hereinafter referred as to periodic KdV solutions and singly periodic KP solutions). Figure 8 shows wave profiles of the periodic KdV solution $H_{\mathrm{KdV}}(T + Y)$ (see Appendix C for details) and superposition of them for parameters $(\varepsilon, \theta, D/2\pi) = (0.01, 85^\circ, 1/200)$. As mentioned earlier the biperiodic KP solution becomes unphysical for large interaction angles θ because the KP equation is derived by choosing the principal direction for wave propagation and assuming weak two-dimensionality. The same is true when it comes to the singly periodic KP solution; therefore, for large interaction angles θ, the superposition of the periodic KdV solution can express more reasonable waves than the singly periodic KP solution does (see figure 4). In this respect, by comparing periodic KdV solutions with singly periodic KP solutions, we may clarify the deficiency due to the weak two-dimensionality approximation of the KP theory. Figure 9 shows the wave frequency W and the maximum wave height α for periodic KdV solutions, singly periodic KP solutions, and biperiodic KP solution. In figure 9, as the interaction angle θ decreases, singly periodic KP solutions deviates from the corresponding periodic KdV solutions; moreover, the singly periodic KP solutions appear to be asymptotic to the biperiodic KP solutions. The deficiency of the biperiodic KP solutions resulting from the weak two-dimensionality approximation is replaced well by the difference between the periodic KdV solutions and the singly periodic KP solutions.

Similar to the correction provided Yeh et al. [1] for KP solitons, we provide the correction that uses $\varepsilon \sin^2 \theta$ instead of the original wave amplitude ε for either biperiodic

or singly periodic KP solutions. One can confirm this by replacing solitons of the hyperbolic function in Yeh et al. [1] with periodic solutions of the Jacobian elliptic function. According to this correction, we modify (23) as follows:

$$\varepsilon D \sin^2\theta - H_{\mathrm{KP}}\left(\frac{\pi}{2}, \frac{\pi}{2}; b, \lambda\right) + H_{\mathrm{KP}}\left(\pi, 0; b, \lambda\right) = 0. \tag{29}$$

Figure 10 and table 3 show results corrected using (29) instead of (23).

Table 3. Results from table 1 corrected using (29).

θ	ε	Case	$W_{\mathrm{dir}} - 1$	$W_{\mathrm{KP}} - 1$	α_{dir}	α_{KP}	$\frac{W_{\mathrm{KP}}}{W_{\mathrm{dir}}} - 1$	$\frac{\alpha_{\mathrm{KP}}}{\alpha_{\mathrm{dir}}} - 1$
45°	0.1	A	3.06×10^{-2}	7.39×10^{-2}	1.81	1.79	4.21×10^{-2}	-1.35×10^{-2}
	0.05	B	1.22×10^{-2}	6.70×10^{-2}	1.64	1.63	5.41×10^{-2}	-6.60×10^{-3}
	0.01	C	8.48×10^{-4}	6.28×10^{-2}	1.23	1.23	6.19×10^{-2}	-3.25×10^{-3}
59.5°	0.1	D	3.50×10^{-2}	3.68×10^{-2}	2.09	2.12	1.70×10^{-3}	1.62×10^{-2}
	0.05	E	1.34×10^{-2}	2.11×10^{-2}	1.76	1.76	7.58×10^{-3}	2.18×10^{-3}
	0.01	F	9.00×10^{-4}	1.27×10^{-2}	1.25	1.25	1.18×10^{-2}	-2.01×10^{-3}
69.5°	0.1	G	6.59×10^{-2}	6.85×10^{-2}	3.28	3.42	2.47×10^{-3}	4.32×10^{-2}
	0.05	H	1.84×10^{-2}	1.88×10^{-2}	2.20	2.22	3.91×10^{-4}	9.86×10^{-3}
	0.01	I	1.04×10^{-3}	3.48×10^{-3}	1.31	1.31	2.44×10^{-3}	-7.66×10^{-4}

In addition to correcting the wave width, the wave frequency needs correction, which is demonstrated by Yeh et al. [1] only for the KP soliton but not for the periodic KP solution. We have yet to find a method to correct the deficiency in the wave frequency of the biperiodic KP solution. The corrected wave frequency of the biperiodic KP solutions still poorly approximate that of direct numerical solutions for small θ; however, it accurately approximates the wave frequency for large θ, and this correction tends to be more effective for large wave amplitude ε. In addition, the correction for the maximum wave height α is highly effective over the whole range $30° \leq \theta \leq 90°$.

If one looks for a weakly nonlinear shallow water wave model that well approximates the wave frequency W and wave velocity both for large and small θ, Benney-Luke (BL) equation can be considered as a good choice. In fact, Milewski et al. [29] compared the wave velocities for symmetric wave solutions to BL with those to KP and KdV, and the results showed that the wave velocities for BL correspond well with those for KP at large θ and with those for KdV at small θ, which is similar to the present results of the wave frequency of direct numerical solutions in figure 10 (a). The good agreement is due to the isotropy of BL equation i.e., no priori approximation of the weakly two-dimensionality, unlike KP equation.

Next, we examine the correction of the wave profile by studying the important parameter σ and wave profile cross sections. Because the wave height H_{KP} is corrected using (29), to make H_{KP} comparable with original the wave height, we renormalize it as $H^*_{\mathrm{KP}} = H_{\mathrm{KP}}/\sin^2\theta$. Table 4 compares the original rms σ with corrected rms σ_{cor}.

θ	ε	Case	σ	$\sigma_{\rm cor}$
	0.1	A	2.54×10^{-1}	1.40×10^{-2}
45°	0.05	B	2.40×10^{-1}	4.33×10^{-3}
	0.01	C	1.68×10^{-1}	2.26×10^{-3}
	0.1	D	1.34×10^{-1}	2.25×10^{-2}
59.5°	0.05	E	1.09×10^{-1}	7.51×10^{-3}
	0.01	F	6.49×10^{-2}	2.36×10^{-3}
	0.1	G	1.56×10^{-1}	4.59×10^{-2}
69.5°	0.05	H	6.45×10^{-2}	1.17×10^{-2}
	0.01	I	2.73×10^{-2}	2.56×10^{-3}

Table 4. Original rms σ and rms $\sigma_{\rm cor}$ corrected using (29) and the renormalization $H^*_{\rm KP} = H_{\rm KP}/\sin^2\theta$ for cases A-I.

Table 4 shows that the accuracy of the biperiodic KP solutions improves for all cases. In most cases, σ decreases by one or two orders of magnitude, and the resulting wave profiles of the direct numerical solutions are indistinguishable from those of the biperiodic KP solutions (see figure 11). These results show clearly that the correction of Yeh et al. [1] is highly effective even for periodic waves and not only for the maximum wave height α but also for wave heights over whole space.

We now consider how this correction improves in terms of the parameter plane (b, λ). Figure 12 shows b and λ before and after the correction for $\varepsilon = 0.01, 0.05$, and 0.1

As we have seen in figure 6, waves at the central peak are unrealistically narrow, and wave troughs flatten with decreasing θ, thus transforming the solutions into solitons. In the limit $b \to 0$, only four terms in (19) [corresponding to $(m_1 = -1, 0)$, $(m_2 = -1, 0)$] become dominant near of the central peak $(T, Y) = (0, 0)$; these solutions asymptotically construct an exact soliton solution. As shown by figure 12, the parameter $|b|$ rapidly decreases with decreasing λ or θ, which unnaturally sharpens the wave profiles. The method of Yeh et al. [1] corrects the discrepancy so as to increase $|b|$ as oblique interaction λ weakens by assuming a smaller wave amplitude $\varepsilon D \sin^2\theta$.

The maximum value on the horizontal axis in figure 12 is the maximum value for the symmetric biperiodic KP solution; that is, $\lambda = 1/\sqrt{2}$, and λ almost reaches the maximum for the largest angle θ, which explains why we find no biperiodic KP solution with larger θ in figure 12. Similarly, no direct numerical solution is found with high accuracy for angles larger than those shown in figure 4, which may be because the solutions already reach almost the largest angles for symmetric direct numerical solutions.

5. Conclusion

We have shown herein how to compute the truncated double Fourier series solution of the fully-nonlinear water wave equation in shallow water. This is done by generalizing the method used by Okamura [2], and allows us to calculate solutions for fairly shallow water and relatively large wave amplitude [for example, $(\varepsilon, D/2\pi) = (0.01, 1/200), (0.1, 1/50)$].

We have also calculated exact biperiodic solutions to the KP equation based on the Riemann theta function by assuming weakly-nonlinear, dispersive, two-dimensional waves. To clarify how the accuracy of the biperiodic KP solution changes when some of the KP approximations are not satisfied, we have compared direct numerical solutions with the corresponding biperiodic KP solutions for various wave amplitudes, wave depths, and interaction angles. This comparison extends the work done by Bryant [7] to fully-nonlinear cases.

As in the results of Bryant [7], we have found that the wave frequency W_{KP} and maximum wave height α_{KP} of KP solutions are greater than those of the corresponding direct numerical solutions, W_{dir} and α_{dir} and that this effect becomes more pronounced with decreasing θ. Moreover, both W and α eventually diverge to infinity at $\theta = 0$, which is a shortcoming of KP solutions. We have also found that the normalized difference $W_{\mathrm{KP}}/W_{\mathrm{dir}} - 1$ is less than $\alpha_{\mathrm{KP}}/\alpha_{\mathrm{dir}} - 1$, which indicates that the wave frequency is less affected by the failure of the weak nonlinearity approximation, which is consistent with perturbation analysis.

Bryant [7] also shows that the central peaks of biperiodic KP solutions are sharper and higher than those of the corresponding solutions to second-order fundamental water wave equations and that this feature becomes more pronounced with decreasing θ. For cases A-I of the present results, cross sections in the Y direction show the same tendency as obtained by Bryant [7]. These results clearly indicate that biperiodic KP solutions cannot model direct numerical solutions both qualitatively and quantitatively when θ is too small (e.g., $\theta = 45^\circ$) to satisfy the two-dimensionality approximation. For relatively large angles, the central peaks of both direct numerical solutions and biperiodic KP solutions become stems that elongate in the Y direction as θ increases, thus indicating that their phases are similarly shifted by strong oblique interactions

Interestingly, at the water depth $D/2\pi = 1/4$, which is the maximum water depth studied here, and for $\varepsilon = 0.01$, the difference $1 - W_{\mathrm{KP}}/W_{\mathrm{dir}}$ deviates by as much as 2.23×10^{-1}, whereas $1 - \alpha_{\mathrm{KP}}/\alpha_{\mathrm{dir}}$ deviates by only 1.47×10^{-2}. In most of these cases, profiles of the biperiodic KP solutions are virtually indistinguishable from those of the direct numerical solutions.

Applying the correction of Yeh et al. [1] to the biperiodic KP solutions makes it clear this correction is effective even for the biperiodic KP solution. However, the corrected wave frequency of the biperiodic KP solutions still poorly approximates that of direct numerical solutions for $\theta \lesssim 45^\circ$, although the wave frequency is accurate for large θ. This correction tends work better for large wave amplitude ε. In addition, the correction

works well for the maximum wave height α over the entire range $30^\circ \leq \theta \leq 90^\circ$. Finally, by simply dividing the wave height by $\sin^2\theta$, we have found that the correction provides excellent results not only for the maximum wave height α but also for wave heights over the whole space. In most cases, as rms σ decreases by one or two orders of magnitude, the resulting wave profiles of the biperiodic KP solutions become indistinguishable from those of the corresponding direct numerical solutions.

The authors would like to acknowledge useful discussions with Dr. H. Tsuji and the financial support by the Green Asia Program in Kyushu University. We also thank three anonymous referees for their comments and suggestions on an earlier version of this manuscript.

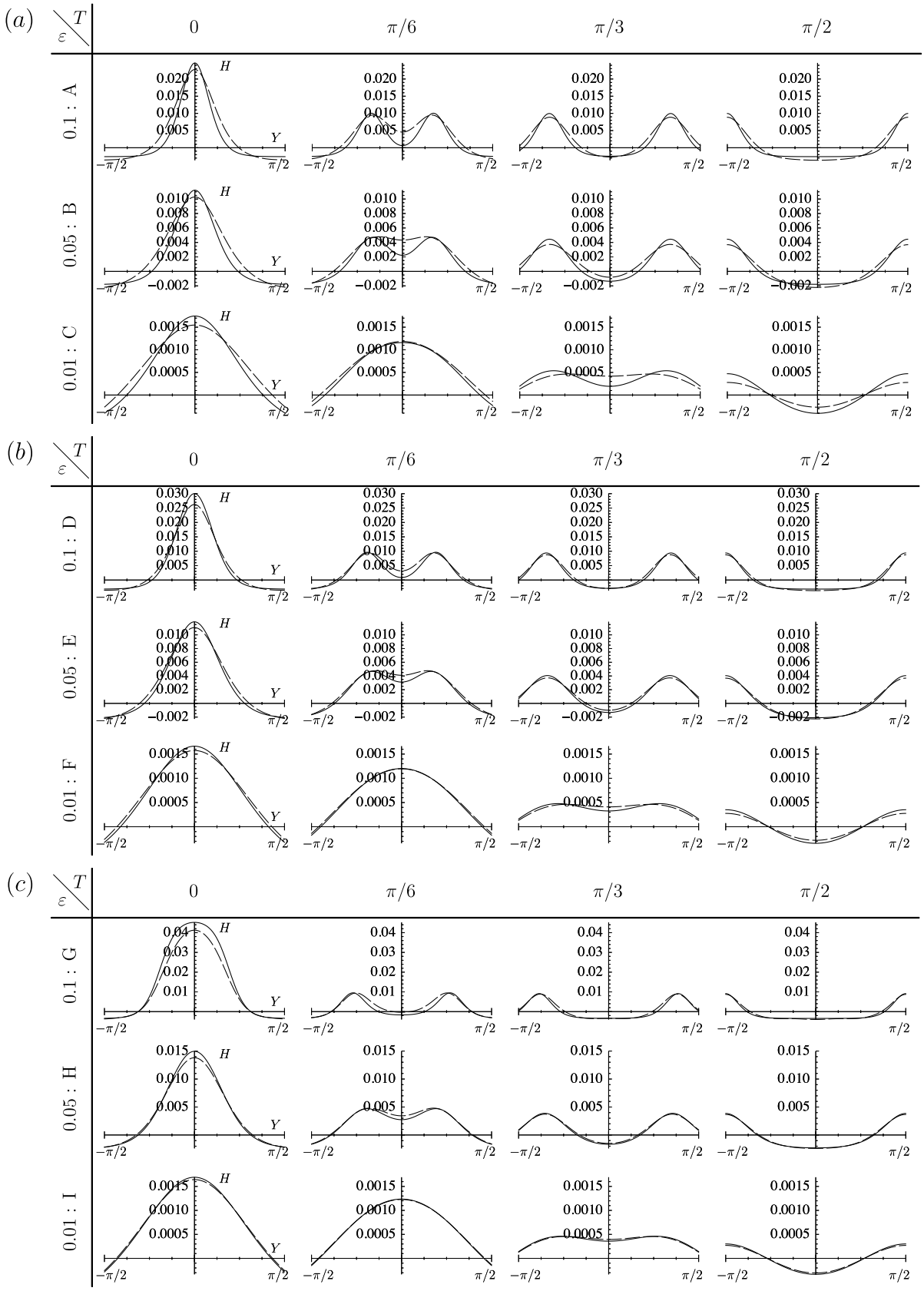

Figure 6. Sequence of wave cross sections from direct numerical solutions (dashed lines) and the biperiodic KP solutions (solid lines) over half a period $-\pi/2 \le Y \le \pi/2$ for $T = 0, \pi/6, \pi/3, \pi/2$ and $\varepsilon = 0.1, 0.05, 0.01$ in shallow water $D/2\pi = 1/50$ with the angle θ fixed at (a) 45°, (b) 59.5°, and (c) 69.5°.

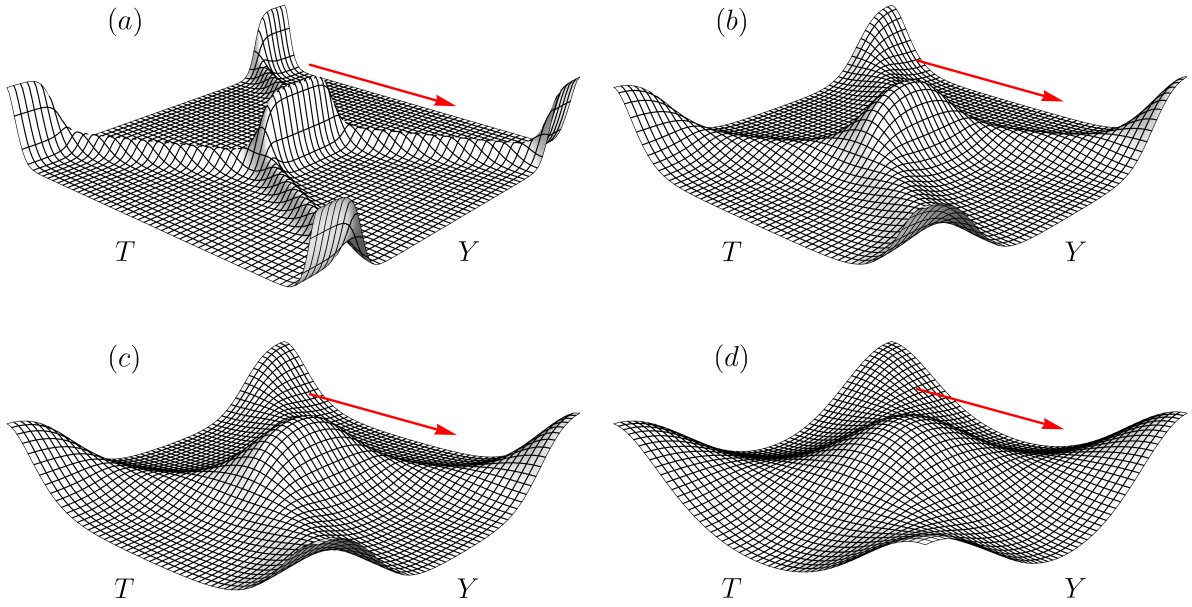

Figure 7. Wave profiles for direct numerical solutions labeled by $\times$ in figures 5(a) and 5(b). The ratio of water depth to wavelength $D/2\pi$ is (a) 1/200, (b) 3/200, (c) 5/200, (d) 7/200, and is thus revealing how a solitary wave lump evolves as the water depth D decreases. The wave profiles of the corresponding biperiodic KP solutions are virtually indistinguishable from these wave profiles shown. To obtain solutions that converge adequately (i.e., $Q < 10^{-4}\varepsilon$), the truncation number N in (11) and the number of samples n for fast Fourier transform in (12) are (a) $(N, n) = (60, 128)$ and (b)-(d) $(N, n) = (50, 64)$.

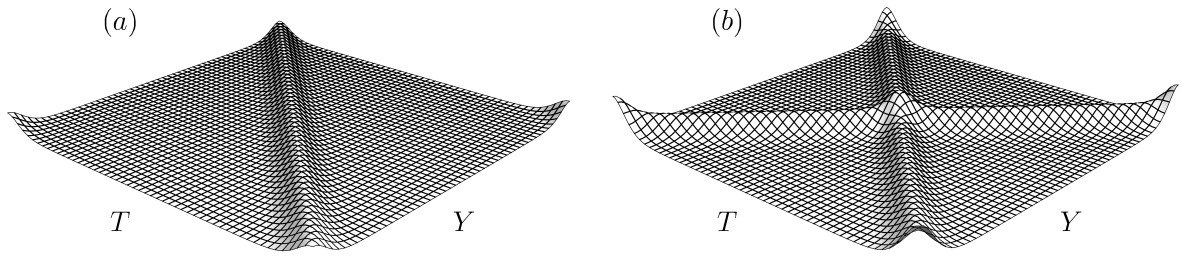

Figure 8. Wave profiles of (a) the periodic KdV solution $H_{\mathrm{KdV}}(T + Y)$ (see Appendix C for details) and (b) superposition of them for parameters $(\varepsilon, \theta, D/2\pi) = (0.01, 85^\circ, 1/200)$ which corresponds with the direct numerical solution shown in figure 7 (a). The superposed wave profile (b) shows no interaction between waves, and this is an example of waves indicated by the symbols $\triangleright$ on vertical axis in figures 4, 9, and 10. For large θ, wave profiles of (a) and (b) are similar to those of singly periodic KP solutions, however only singly periodic KP solutions unnaturally narrow as θ decreases.

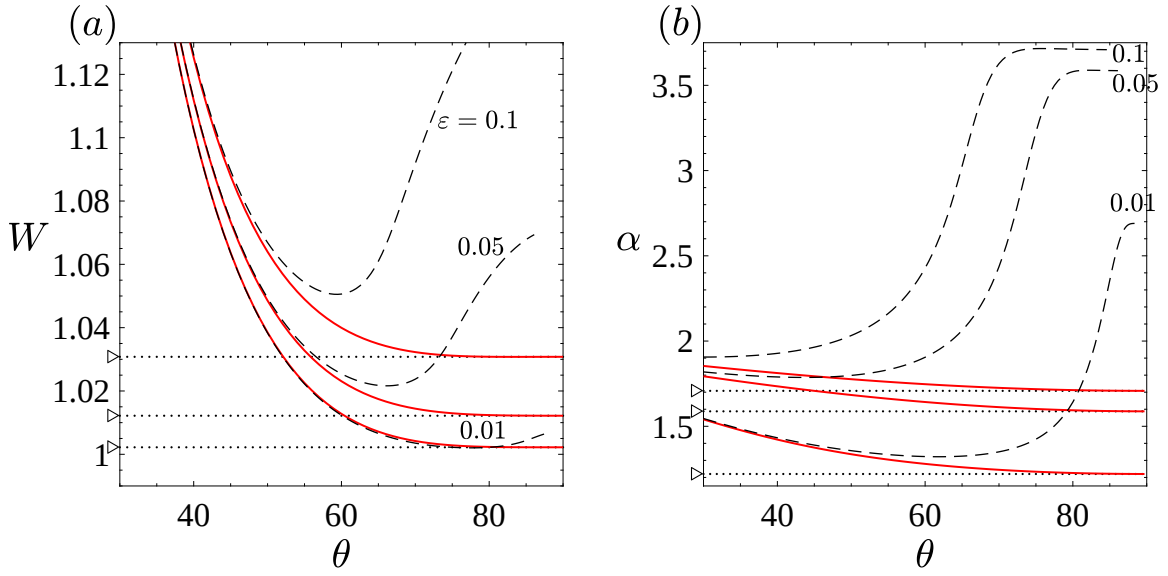

Figure 9. Biperiodic KP solutions (dashed lines), singly periodic KP solutions (solid lines), and periodic KdV solutions (dots) for $\varepsilon = 0.01, 0.05, 0.1$ respectively, showing how (a) wave frequency W and (b) maximum wave height α depend on θ. The symbols $\triangleright$ on the vertical axis indicate the superposition of periodic KdV solutions. Since both singly periodic KP solutions, and periodic KdV solutions involve no oblique interactions, W and α do not increase for large θ.

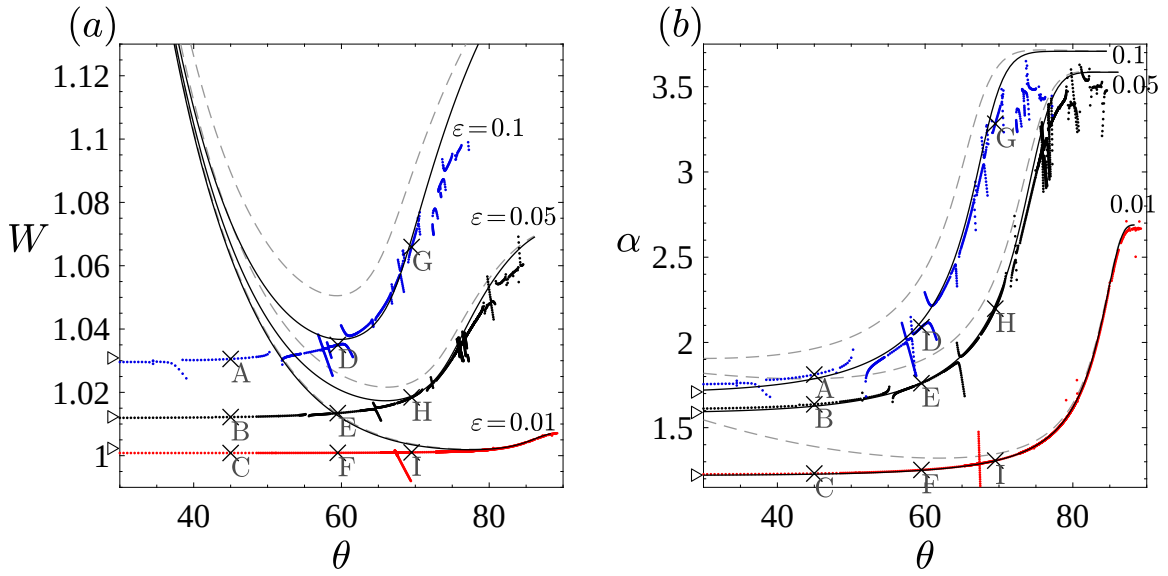

Figure 10. Results from figure 4 corrected using (29) (solid lines), direct solutions (dots), and biperiodic KP solutions (dashed lines) for $\varepsilon = 0.01$ (bottom), 0.05 (middle), and 0.1 (top), showing how (a) wave frequency W and (b) maximum wave height α depend on θ. The symbols $\times$ indicate direct numerical solutions for cases A-I, and the symbols $\triangleright$ on the vertical axis indicate the superposition of periodic KdV solutions.

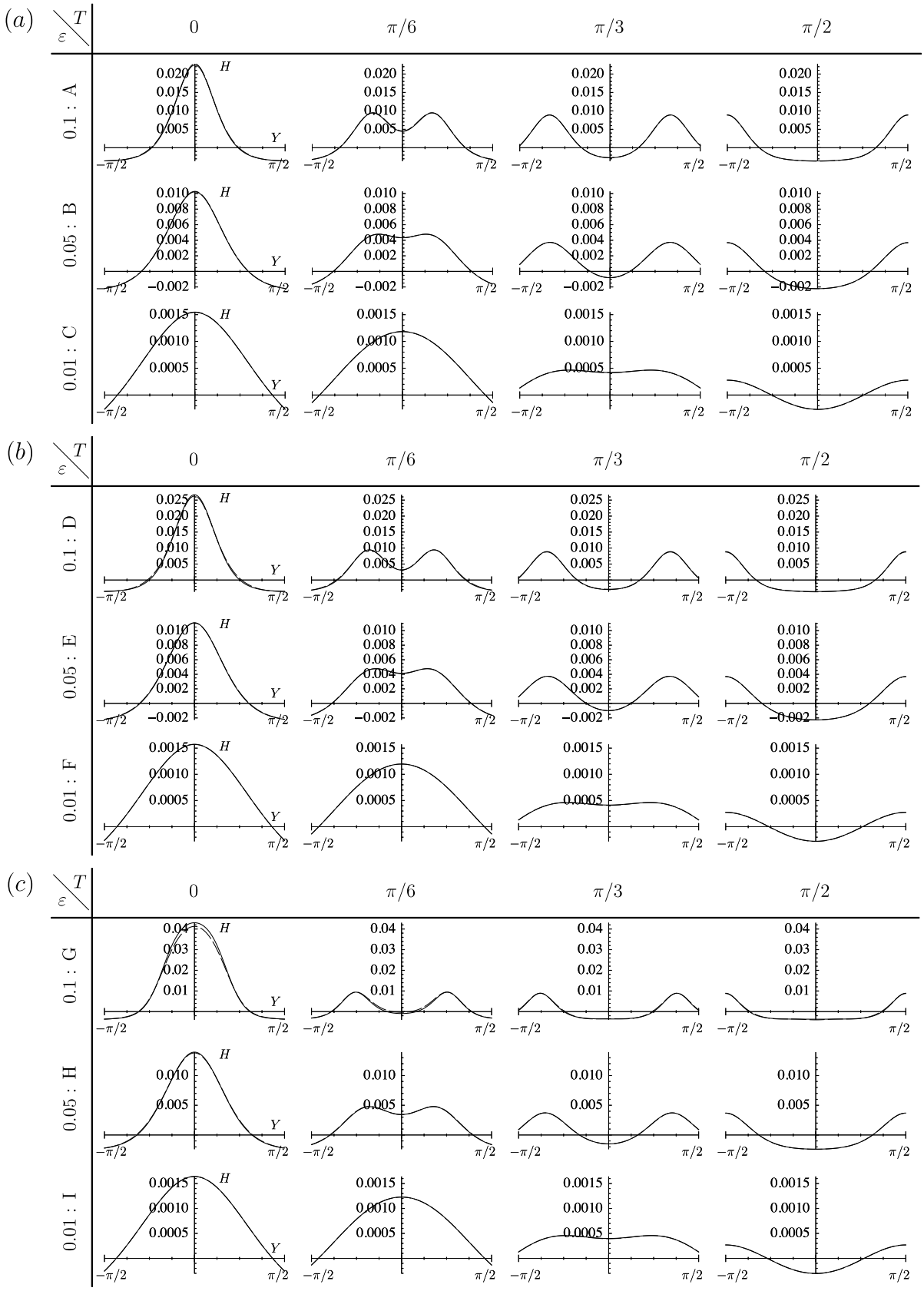

Figure 11. Sequence of wave cross sections from direct numerical solutions (dashed lines) and the corrected biperiodic KP solutions (solid lines) over half a period $-\pi/2 \le Y \le \pi/2$ for $T = 0, \pi/6, \pi/3, \pi/2$ and $\varepsilon = 0.1, 0.05, 0.01$ in shallow water $D/2\pi = 1/50$ with the angle θ fixed at (a) 45°, (b) 59.5°, and (c) 69.5°.

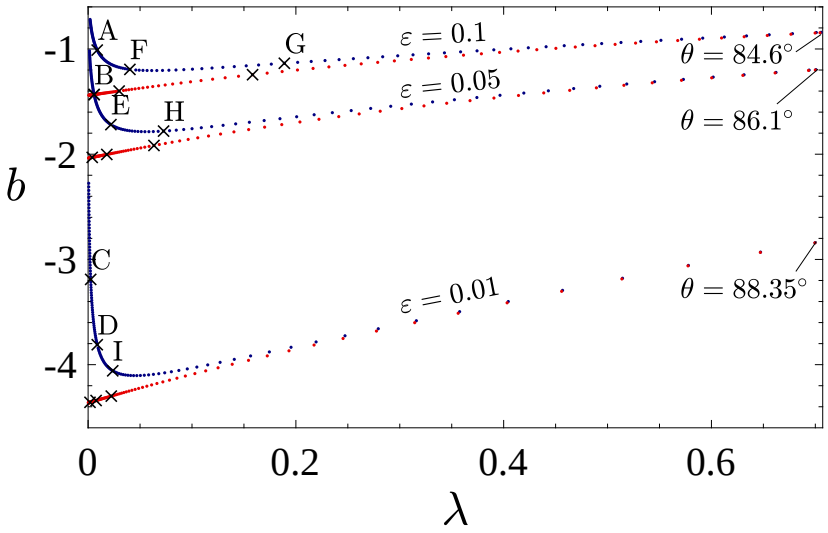

Figure 12. Parameter plane (b, λ) for the biperiodic KP solutions, before (upper dots for each ε) and after (lower dots for each ε) the correction for $\varepsilon = 0.01, 0.05, 0.1$ and $D/2\pi = 1/50$. For each ε, dots are at intervals of $\theta = 0.5°$ except for the largest θ. The symbols $\times$ denote solutions of cases A-I.

Appendix A. A Jacobian matrix

Here, we show how to calculate the elements of the Jacobian matrix

$$J = \begin{bmatrix} \frac{\partial F_{l,m}}{\partial A_{j,k}} & \frac{\partial F_{l,m}}{\partial B} & \frac{\partial F_{l,m}}{\partial G} \\ \frac{\partial s}{\partial A_{j,k}} & \frac{\partial s}{\partial B} & \frac{\partial s}{\partial B} \\ \frac{\partial \Pi}{\partial A_{j,k}} & \frac{\partial \Pi}{\partial B} & \frac{\partial \Pi}{\partial G} \end{bmatrix}. \tag{A.1}$$

Because no information is available on the derivatives of the wave height H, we evaluate the derivatives by using, for example, the derivatives of (9):

$$\frac{\partial H}{\partial A_{j,k}} = -\frac{\partial P/\partial A_{j,k}}{\partial P/\partial Z}\bigg|_{Z=H(T,Y)}. \tag{A.2}$$

In a similar manner, we can calculate each element of J as

$$\frac{\partial F_{l,m}}{\partial A_{j,k}} = \int_0^\pi dT \int_0^\pi dY \left(\frac{\partial Q}{\partial A_{j,k}} - \frac{\partial Q}{\partial Z}\frac{\partial P/\partial A_{j,k}}{\partial P/\partial Z} \right)\bigg|_{Z=H(T,Y)} \cos(lY)\sin(mT), \tag{A.3}$$

$$\frac{\partial F_{l,m}}{\partial B} = \int_0^\pi dT \int_0^\pi dY \left(-\frac{\partial Q/\partial Z}{\partial P/\partial Z} \right)\bigg|_{Z=H(T,Y)} \cos(lY)\sin(mT), \tag{A.4}$$

$$\frac{\partial F_{l,m}}{\partial G} = \int_0^\pi dT \int_0^\pi dY \left(\frac{\partial Q}{\partial G} - \frac{\partial Q}{\partial Z}\frac{\partial P/\partial G}{\partial P/\partial Z} \right)\bigg|_{Z=H(T,Y)} \cos(lY)\sin(mT), \tag{A.5}$$

$$\frac{\partial s}{\partial A_{j,k}} = -\int_0^\pi dT \int_0^\pi dY \frac{\partial P/\partial A_{j,k}}{\partial P/\partial Z}\bigg|_{Z=H(T,Y)}, \tag{A.6}$$

$$\frac{\partial s}{\partial G} = -\int_0^\pi dT \int_0^\pi dY \frac{\partial P/\partial G}{\partial P/\partial Z}\bigg|_{Z=H(T,Y)}, \tag{A.7}$$

$$\frac{\partial s}{\partial B} = -\int_0^\pi dT \int_0^\pi dY \frac{1}{\partial P/\partial Z}\bigg|_{Z=H(T,Y)}, \tag{A.8}$$

$$\frac{\partial \Pi}{\partial A_{j,k}} = \frac{\partial P/\partial A_{j,k}}{\partial P/\partial Z}\bigg|_{(T,Y,Z)=(\pi/2,\pi/2,H)} - \frac{\partial P/\partial A_{j,k}}{\partial P/\partial Z}\bigg|_{(T,Y,Z)=(0,\pi,H)}, \tag{A.9}$$

$$\frac{\partial \Pi}{\partial G} = \frac{\partial P/\partial G}{\partial P/\partial Z}\bigg|_{(T,Y,Z)=(\pi/2,\pi/2,H)} - \frac{\partial P/\partial G}{\partial P/\partial Z}\bigg|_{(T,Y,Z)=(0,\pi,H)}, \tag{A.10}$$

$$\frac{\partial \Pi}{\partial B} = \frac{1}{\partial P/\partial Z}\bigg|_{(T,Y,Z)=(\pi/2,\pi/2,H)} - \frac{1}{\partial P/\partial Z}\bigg|_{(T,Y,Z)=(0,\pi,H)}. \tag{A.11}$$

Appendix B. Determination of parameters for the biperiodic KP solution

To set a point of the maximum wave height at the center $(T, Y) = (0, 0)$, Θ is already shifted by π in (19). For symmetric waves, the parameters satisfy

$$(M_1, N_1, \Omega_1) = (M_2, -N_2, \Omega_2), \quad d = b\left(1 - \lambda^2\right). \tag{B.1}$$

Besides the less important two phase parameters, we have nine parameters $b, \lambda, d, M_1, M_2, N_1, N_2, \Omega_1, \Omega_2$. By using (B.1), we reduce the number of parameters to five: $b, \lambda, M_1, N_1, \Omega_1$. To fix the period of solutions to 2π, we have set $(M_1, N_1) =$

$(D\sin\theta, D\cos\theta)$ where D and θ are already defined in (6) and below (6). The solution (19) satisfies (17) if and only if parameters satisfy the four equations indexed by two component vectors $\mathbf{p}_i$. In the case for symmetric wave cases, these four equations can be written as

$$\mathbf{M}\cdot\mathbf{X} = 4\mathbf{S}\cdot\mathbf{V}, \tag{B.2}$$

where

$$\mathbf{X} = (\Omega_1\mathbf{Y}_1 + \mathbf{Y}_2, C)^{\mathsf{T}}, \quad \mathbf{V} = M_1^4\big(1, 4(1-\lambda), 6(1-\lambda)^2, 4(1-\lambda)^3, (1-\lambda)^4\big)^{\mathsf{T}},$$

$$\mathbf{M} = \begin{pmatrix} \mathbf{M}_1 & \hat{\vartheta}(\mathbf{p}_4) \\ \vdots & \vdots \\ \mathbf{M}_4 & \hat{\vartheta}(\mathbf{p}_4) \end{pmatrix}, \quad \mathbf{S} = \begin{pmatrix} \mathbf{S}_1 \\ \vdots \\ \mathbf{S}_4 \end{pmatrix}.$$

Here, C is an integral constant,

$$\mathbf{Y}_1 = M_1\big(1, 2(1-\lambda), (1+\lambda)^2\big), \quad \mathbf{Y}_2 = 3N_1^2\big(1, -2(1+\lambda), (1+\lambda)^2\big),$$

$$\mathbf{M}_i = \left(\frac{\partial\hat{\vartheta}(\mathbf{p}_i)}{\partial b}, \frac{1}{2b}\frac{\partial\hat{\vartheta}(\mathbf{p}_i)}{\partial\lambda}, \frac{\partial\hat{\vartheta}(\mathbf{p}_i)}{\partial d}\right), \quad (i=1,\ldots,4),$$

$$\mathbf{S}_i = \left(\frac{\partial^2\hat{\vartheta}(\mathbf{p}_i)}{\partial b^2}, \frac{\partial}{\partial b}\left(\frac{1}{2b}\frac{\partial\hat{\vartheta}(\mathbf{p}_i)}{\partial\lambda}\right), \frac{\partial^2\hat{\vartheta}(\mathbf{p}_i)}{\partial b\partial d}, \frac{1}{2b}\frac{\partial^2\hat{\vartheta}(\mathbf{p}_i)}{\partial d\partial\lambda}, \frac{\partial^2\hat{\vartheta}(\mathbf{p}_i)}{\partial d^2}\right), \quad (i=1,\ldots,4).$$

The theta constant is given as

$$\hat{\vartheta}(\mathbf{p}_i) = \sum_{m_1=-\infty}^{\infty}\sum_{m_2=-\infty}^{\infty} \exp\Big[(\mathbf{m}+\mathbf{p}_i)^{\mathsf{T}}\cdot\mathbf{B}\cdot(\mathbf{m}+\mathbf{p}_i)\Big], \quad (i=1,\ldots,4), \tag{B.3}$$

where $\mathbf{p}_1 = (0,0)^{\mathsf{T}}$, $\mathbf{p}_2 = (1/2,0)^{\mathsf{T}}$, $\mathbf{p}_3 = (0,1/2)^{\mathsf{T}}$, $\mathbf{p}_4 = (1/2,1/2)^{\mathsf{T}}$, and the vector $\mathbf{m}$ is defined in (19). Here, $\hat{\vartheta}(\mathbf{p}_2)$ is equivalent to $\hat{\vartheta}(\mathbf{p}_3)$. (B.2) is arranged as

$$\mathbf{M}_i\cdot(\Omega_1\mathbf{Y}_1 + \mathbf{Y}_2) + C\hat{\vartheta}(\mathbf{p}_i) = 4\mathbf{S}_i\cdot\mathbf{V}, \quad (i=1,2,4). \tag{B.4}$$

Eliminating C from (B.4), Ω_1 is written as

$$\Omega_1 = \frac{4\Big(\mathbf{S}_i\hat{\vartheta}(\mathbf{p}_j) - \mathbf{S}_j\hat{\vartheta}(\mathbf{p}_i)\Big)\cdot\mathbf{V} - \Big(\mathbf{M}_i\hat{\vartheta}(\mathbf{p}_j) - \mathbf{M}_j\hat{\vartheta}(\mathbf{p}_i)\Big)\cdot\mathbf{Y}_2}{\Big(\mathbf{M}_i\hat{\vartheta}(\mathbf{p}_j) - \mathbf{M}_j\hat{\vartheta}(\mathbf{p}_i)\Big)\cdot\mathbf{Y}_1}. \tag{B.5}$$

Without loss of generality, we choose indices $(i,j) = (1,2)$ for Ω_1 and $(i,j) = (1,4)$ for Ω_2, and we obtain relation (20) between the parameters b and λ.

Appendix C. Determination of parameters for KP and KdV solutions of Jacobian elliptic function

The singly periodic KP solution to (17) can be written as

$$U(\hat{X},\hat{Y},\hat{T}) = A\,\mathrm{dn}^2(\Theta;m) + U_0, \quad \Theta = M\hat{X} + N\hat{Y} + \Omega\hat{T}. \tag{C.1}$$

Here, we determine parameters A, M, N, Ω, U_0 based on direct numerical solutions. The Jacobian elliptic function $\mathrm{dn}(\Theta; m)$ is defined as

$$x = \mathrm{dn}(\Theta; m), \quad \mathrm{dn}^{-1}(x; m) = \Theta = \int_x^1 \frac{dx}{\sqrt{(1-x^2)\,(x^2+m-1)}},$$

which has a period of $2K(m)$, where $K(m)$ is the complete elliptic integral of the first kind, and m is the modulus. For the singly periodic KP solution, the amplitude A and dispersion relation become

$$A = 2M^2, \quad \frac{\Omega}{M} = -4M^2\,(2-m) - 6U_0 - 3\left(\frac{N}{M}\right)^2. \tag{C.2}$$

Setting M, N so that the period of the solutions is 2π in both direction $\hat{X}, \hat{Y}$ gives

$$(M, N) = \left(\frac{K(m)}{\pi} D \sin\theta, \frac{K(m)}{\pi} D \cos\theta\right). \tag{C.3}$$

where D is the non-dimensional mean water depth in (6). Similarly to (21), we consider the free-surface displacement of a traveling wave U^* on the moving coordinate system T^* and define the wave height of singly periodic KP solution:

$$\begin{aligned} &H_{\mathrm{sKP}}(T, Y) = \frac{2D}{3} U^*\left(\frac{K(m)}{\pi} T, \frac{K(m)}{\pi} Y\right), \\ &U^*(T^*, \hat{Y}) = U(\hat{X}, \hat{Y}, \hat{T}), \quad T^* = \hat{X} + \frac{\Omega}{M}\hat{T}. \end{aligned} \tag{C.4}$$

Using $\mathrm{dn}^2(0; m) = 1$ and $\mathrm{dn}^2(K(m); m) = 1 - m$, the relation that corresponds to (14) becomes

$$\varepsilon - \frac{4}{3} m M^2 = 0. \tag{C.5}$$

We solve (C.5) for the modulus m. Note that $K(m)$ has logarithmic singularity at $m = 1$, and the convergence of the hypergeometric series to compute $K(m)$ becomes slow with increasing m; therefore, we first transform variable by using $m = 1 - \exp(-w)$, and we recover m after computing w [30]. The relation that corresponds to (13) is

$$AE\,(m) + U_0 K\,(m) = 0. \tag{C.6}$$

Here, we used the formula

$$\int_0^{2K(m)} \mathrm{dn}\,(\Theta; m)\, d\Theta = E\,(m)\,,$$

where $E\,(m) = E\,(\pi/2; m)$ is the complete elliptic integral of the second kind. The wave frequency W_{sKP} and the maximum wave height α_{sKP} of the singly periodic KP solutions are

$$\alpha_{\mathrm{sKP}} = H_{\mathrm{sKP}}(0, 0)/D, \tag{C.7}$$

$$W_{\mathrm{sKP}} = \sin\theta \left(1 + \varepsilon\left(\frac{1}{m} - \frac{1}{2} - \frac{3\varepsilon}{2}\frac{E\,(m)}{K\,(m)}\right) + \frac{1}{2}\cot^2\theta\right). \tag{C.8}$$

The periodic KdV solutions $H_{\mathrm{KdV}}(T)$ can be calculated in a similar manner setting $\theta = 90°$.

References

[1] Yeh H, Li W and Kodama Y 2010 Eur. Phys. J. Spec. Top. **185** 97–111 ISSN 1951-6355 (*Preprint* 1004.0370) URL http://arxiv.org/abs/1004.0370 http://www.springerlink.com/index/10.1140/epjst/e2010-01241-0

[2] Okamura M 2010 J. Fluid Mech. **646** 481–503 ISSN 0022-1120 URL http://www.journals.cambridge.org/abstract_S0022112009992795

[3] Tsai C P, Jeng D and Hsu J R C 1994 Appl. Ocean Res. **16** 317–326 ISSN 01411187 URL http://linkinghub.elsevier.com/retrieve/pii/0141118794000212

[4] Ioualalen M, Okamura M, Cornier S, Kharif C and Roberts A J 2006 J. Waterw. Port, Coastal, Ocean Eng. **132** 157–165 ISSN 0733-950X URL http://ascelibrary.org/doi/10.1061/%2528ASCE%25290733-950X%25282006%2529132%253A3%2528157%2529

[5] Roberts A J 1983 J. Fluid Mech. **135** 301–321 ISSN 0022-1120 URL http://www.journals.cambridge.org/abstract_S0022112083003092

[6] Ioualalen M, Roberts A J and Kharif C 1996 J. Fluid Mech. **322** 1 ISSN 0022-1120 URL http://www.journals.cambridge.org/abstract_S0022112096002686

[7] Bryant P J 1982 J. Fluid Mech. **115** 525–532 ISSN 0022-1120 URL http://www.journals.cambridge.org/abstract_S0022112082000895

[8] Marchant T R and Roberts A J 1987 J. Aust. Math. Soc. Ser. B. Appl. Math. **29** 103–125 ISSN 0334-2700 URL http://www.journals.cambridge.org/abstract_S0334270000005658

[9] Fenton J D and Rienecker M M 1982 J. Fluid Mech. **118** 411 ISSN 0022-1120 URL http://journals.cambridge.org/abstract_S0022112082001141 http://www.journals.cambridge.org/abstract_S0022112082001141

[10] Hsu J R C, Tsuchiya Y and Silvester R 1979 J. Fluid Mech. **90** 179–196 ISSN 0022-1120 URL http://www.journals.cambridge.org/abstract_S0022112079002135

[11] Nicholls D P and Reitich F 2006 Eur. J. Mech. B/Fluids **25** 406–424 ISSN 09977546 URL http://linkinghub.elsevier.com/retrieve/pii/S0997754605001020

[12] Nicholls D P and Reitich F 2005 Proc. R. Soc. A Math. Phys. Eng. Sci. **461** 1283–1309 ISSN 1364-5021 URL http://rspa.royalsocietypublishing.org/content/royprsa/461/2057/1283.full.pdf http://rspa.royalsocietypublishing.org/cgi/doi/10.1098/rspa.2004.1427

[13] Roberts A J and Schwartz L W 1983 Phys. Fluids **26** 2388–2392 ISSN 00319171 URL http://scitation.aip.org/content/aip/journal/pof1/26/9/10.1063/1.864422

[14] Okamura M 1996 J. Phys. Soc. Jpn **65** 2841–2845 ISSN 0031-9015 URL http://journals.jps.jp/doi/abs/10.1143/JPSJ.65.2841

[15] Tsai C P and Jeng D S 1994 Appl. Ocean Res. **16** 185–193 ISSN 01411187 URL http://linkinghub.elsevier.com/retrieve/pii/0141118794900280

[16] Kadomtsev B B and Petviashvili V I 1970 Sov. Phys. Dokl. **15** 539–541

[17] Dubrovin B A 1981 Russ. Math. Surv. **36** 11–92 ISSN 0036-0279 URL http://stacks.iop.org/0036-0279/36/i=2/a=R02?key=crossref.10a0e70699918ea6c4a821859b580c01

[18] Nakamura A 1979 J. Phys. Soc. Jpn **47** 1701–1705 URL http://journals.jps.jp/doi/pdf/10.1143/JPSJ.47.1701

[19] Segur H and Finkel A 1985 Stud. Appl. Math. **73** 183–220 ISSN 00222526 URL http://doi.wiley.com/10.1002/sapm1985733183

[20] Akylas T R 1994 Annu. Rev. Fluid Mech. **26** 191–210 ISSN 0066-4189 URL http://www.annualreviews.org/doi/10.1146/annurev.fl.26.010194.001203

[21] Hammack J L 1989 J. Fluid Mech. **209** 567–589 URL http://journals.cambridge.org/abstract_S0022112089003228

[22] Miles J W 1977 J. Fluid Mech. **79** 157–167 ISSN 0022-1120 URL http://www.journals.cambridge.org/abstract_S0022112077000081

[23] Miles J W 1977 J. Fluid Mech. **80** 149 ISSN 0022-1120 URL http://www.journals.cambridge.org/abstract_S0022112077001578

[24] Li W, Yeh H and Kodama Y 2011 J. Fluid Mech. **672** 326–357 ISSN 0022-1120 URL http://www.journals.cambridge.org/abstract_S0022112010006014
[25] Funakoshi M 1980 J. Phys. Soc. Jpn ISSN 0031-9015
[26] Tanaka M 1993 J. Fluid Mech. **248** 637 ISSN 0022-1120 URL http://journals.cambridge.org/abstract_S0022112093000941 http://www.journals.cambridge.org/abstract_S0022112093000941
[27] Okamura M 2003 Wave Motion **37** 173–182 ISSN 01652125 URL http://linkinghub.elsevier.com/retrieve/pii/S0165212502000550
[28] Roberts A J and Peregrine D H 1983 J. Fluid Mech. **135** 323–335 ISSN 0022-1120 URL http://www.journals.cambridge.org/abstract_S0022112083003109
[29] Milewski P A and Keller J B 1996 Stud. Appl. Math. **97** 149–166 ISSN 00222526 URL http://doi.wiley.com/10.1002/sapm1996972149
[30] Fukushima T 2013 J. Comput. Appl. Math. **249** 37–50 ISSN 03770427 URL http://linkinghub.elsevier.com/retrieve/pii/S0377042713000630